ACS OMEGA

Open Access

http://pubs.acs.org/journal/acsodf

Article

Tryptophan End-Tagging Confers Antifungal Activity on a Tick-Derived Peptide by Triggering Reactive Oxygen Species Production

Court K. Chiramba, Dalton S. Möller, Christian D. Lorenz, Rumbidzai R. Chirombo, A. James Mason, Megan J. Bester, and Anabella R. M. Gaspar*

Cite This: *ACS Omega* 2024, 9, 15556−15572

Read Online

ACCESS | Metrics & More | Article Recommendations | Supporting Information

ABSTRACT: WHO has identified several *Candida* species including *Candida albicans* as critical priority fungal pathogens due to greater infection prevalence and formation of recalcitrant biofilms. Novel antifungal agents are urgently needed, and antimicrobial peptides (AMPs) are being considered as potential alternatives, but inactivity in physiological salt environments, serum, and plasma often limits further therapeutic development. Tryptophan end-tagging is a strategy to overcome these limitations and is thought to selectively enhance membrane permeabilization in both fungal and bacterial plasma membranes. Here, we show that C-terminal tryptophan end-tagging of the tick-derived peptide Os−C transforms an inactive peptide into Os−C(W_5), an antifungal peptide capable of preventing the formation of *C. albicans* biofilms. Mechanistic insight is provided by circular dichroism spectroscopy and molecular dynamics simulations, which demonstrate that tryptophan end-tagging alters the secondary structure of Os−C, while the latter reveals that end-tagging reduces interactions with, and insertion into, a model *C. albicans* membrane but promotes peptide aggregation on its surface. Interestingly, this leads to the induction of reactive oxygen species production rather than membrane permeabilization, and consequently, oxidative stress leads to cell wall damage. Os−C(W_5) does not induce the hemolysis of human erythrocytes. Reduced cell adhesion and viability contribute to decreased biofilm extracellular matrix formation which, although reduced, is retained in the serum-containing medium. In this study, tryptophan end-tagging was identified as a promising strategy for enhancing the antifungal activity, including the biofilm inhibitory activity of Os−C against *C. albicans* in physiological salt environments.

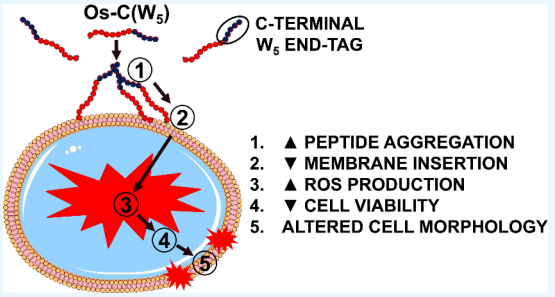

INTRODUCTION

In October 2022, the World Health Organization identified *Cryptococcus neoformans*, *Aspergillus fumigatus*, *Candida albicans*, and *Candida auris* as "critical" priority fungal pathogens.[1] The presence of two *Candida* species indicates that this fungus is a serious public health threat due to the formation of difficult to treat biofilms associated with superficial mucosal or invasive systemic infections such as candidemia, peritonitis, and osteomyelitis.[2]

Three classes of antifungal drugs are currently used in antifungal therapy: polyenes, azoles, and echinocandins;[3] however, the emergence of resistant isolates is increasing and is of concern. Several studies in Africa have identified resistant isolates,[4−6] and a study by the WHO noted that 49% of *Candida* clinical isolates were resistant to fluconazole.[7] The development of drug resistance is associated with an increase in efflux pumps or the modification of specific drug targets.[8] In addition, established biofilms are difficult to treat because of the extracellular matrix (ECM) which acts as a physical barrier that provides cellular protection, reduces the rate of drug diffusion, and binds antifungal drugs.[9] Increasing antifungal resistance coupled with the toxic side effects associated with antifungal drug treatment underscores the need for novel antifungal agents.

Antimicrobial peptides (AMPs), key components of the innate immune systems of living organisms,[10] are considered as potential alternatives or as leads for the development of new antifungal drugs. Most AMPs are short (12−50 amino acids), cationic, and amphipathic, have broad-spectrum activity, and possess multiple modes of cell killing.[11] To date, with varying degrees of success, numerous AMPs are being evaluated in clinical trials for various infections.[12] Recently, the lipopeptide rezafungin was approved by the United States Food and Drug Administration for the treatment of candidemia and invasive candidiasis.[13]

Despite their potential, major drawbacks to the further development of many active AMPs are the susceptibility to

Received: January 15, 2024
Revised: February 26, 2024
Accepted: March 7, 2024
Published: March 19, 2024

proteases and inactivity in the presence of salt, serum, and plasma.[14] Strategies to increase activity in a physiological salt environment include the incorporation of unnatural amino acids such as β-naphtylalanine and β-(4,4′-biphenyl)alanine[15] and end-tagging with hydrophobic amino acids such as phenylalanine and tryptophan.[16,17] Several studies have shown that the latter strategy has led to increased antimicrobial activity and selectivity for bacterial and fungal membrane liposomes, with activity being retained in the presence of salts, serum, and plasma.[16−21] Addition of tryptophan end-tags led to greater peptide-induced permeabilization of bacterial cell membranes,[16] bacterial liposomes,[16−19] and fungal liposomes[19,21] compared with nontagged peptides. Furthermore, tagged peptides retained their membrane and liposome permeabilizing activity in the presence of 0.15 M NaCl.[16−20] Tryptophan end-tagging of the peptide GKH17, with three tryptophan residues either on the C- or N-terminal, led to improved activity against *Escherichia coli*, *Staphylococcus aureus*, and *C. albicans* , and activity against *E. coli* in the presence of 0.15 M NaCl was retained.[17] Increased activity of the tryptophan end-tagged GKH17 against *C. parapsilosis* was also observed in 0.15 M NaCl, 50% human plasma, and 50% human serum compared with the nontagged parent peptide.[21] Although these studies[16−21] investigated interactions between tagged peptides and liposomes, it is not clear how end-tagging affects peptide-membrane interactions. Therefore, using molecular dynamics (MD) simulations, this interaction with a model fungal membrane was investigated in this study. Typically, assessment of the antimicrobial activity of tryptophan end-tagged peptides is evaluated against planktonic bacteria and fungi; however, there is a notable absence of studies investigating whether the same antimicrobial effect extends to biofilms.

Several studies have investigated the antibacterial[22,23] and antifungal[24] activities of a synthetic peptide Os−C, a derivative of a defensin OsDef2, identified in the midgut of the soft tick *Ornithodoros savignyi*. Although Os−C possessed antiplanktonic activity, its activity could only be determined in sodium phosphate buffer (NaP), pH 7.4. Under these conditions, mode of action studies revealed that Os−C interacted with the cell wall polysaccharides mannan and laminarin but did not cause membrane permeabilization. Confocal microscopy images showed that Os−C entered the cytoplasm via an energy-dependent mechanism and induced reactive oxygen species (ROS) production which was linked to its antiplanktonic activity.[24] Further development of the use of Os−C as an antifungal agent is limited due to the loss of activity in physiological salt environments. To improve antifungal activity in physiologically relevant salt environments, we have modified Os−C by tagging the C-terminus with five tryptophan residues to create Os−C(W_5).

In this study, the effect of tryptophan tagging on the secondary structure and the interaction of Os−C(W_5) with a model fungal membrane was compared with the parent peptide Os−C. Activity of Os−C(W_5) against planktonic *C. albicans* was determined, the mode of action was elucidated, and the effects of exposure on the *C. albicans* cell wall ultrastructure was evaluated. Further, biofilm inhibitory and eradication studies were undertaken, and activity in serum-containing media was evaluated with the overall purpose being to further develop this peptide for clinical applications.

RESULTS AND DISCUSSION

Tryptophan End-Tagging Alters the Secondary Structure of Os−C. Circular dichroism (CD) spectroscopy was performed to investigate the secondary structures of Os−C and Os−C(W_5) in either Tris buffer or sodium dodecyl sulfate (SDS) (Figure 1).

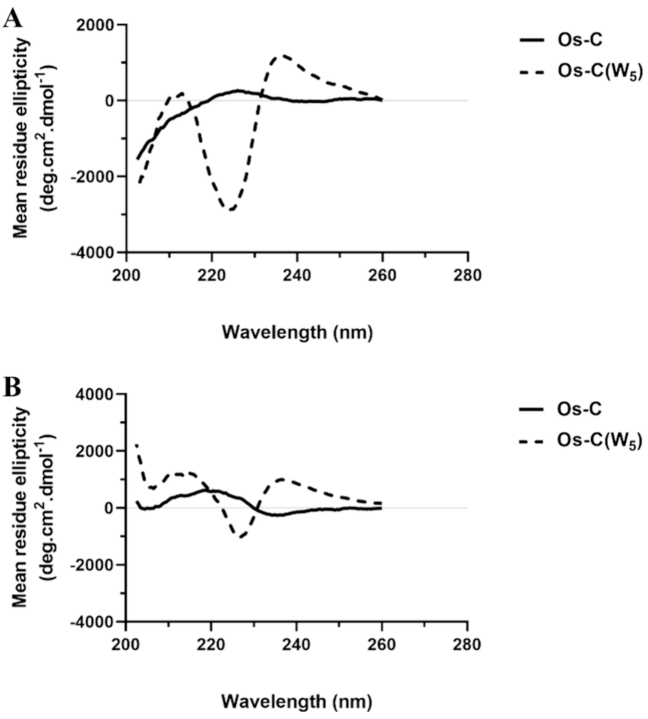

Figure 1. CD spectra of Os−C and Os−C(W_5). CD spectra were determined in either (A) Tris buffer (5 mM) or (B) SDS (50 mM). Mean residue ellipticity values of Os−C and Os−C(W_5) were determined between 180 and 260 nm. CD spectra shown start at 200 nm due to a high-tension voltage above 600 V which resulted in significant background noise.

The CD spectra of Os−C in Tris buffer and SDS in this study are consistent with the spectra obtained by Prinsloo et al. in water and SDS.[22] In contrast, the CD spectra of Os−C(W_5) differ from those of Os−C in both Tris buffer and SDS (Figure 1A,B). The presence of a negative band in the CD spectra of Os−C(W_5) in Tris at 224 nm indicates that tryptophan residues alter the CD signal of Os−C(W_5) (Figure 1A). Tryptophan end-tagging has been found to alter the CD spectra of peptides in the 220−230 nm region.[17,19,20] The peptides KNK7W5, K7W5, and R7W5 all displayed identical CD spectra in Tris buffer with a negative band observed at 225 nm.[20] Likewise, a negative band between 220 and 230 nm in Tris was observed for GRR10W4N.[19]

To mimic a membrane environment, the anionic detergent SDS was used, and the negative band of the Os−C(W_5) spectrum shifts slightly from 224 to 226.5 nm and the minima is diminished by 64% in the presence of SDS (Figure 1B). Strömstedt et al. saw a similar, albeit relatively larger shift, in the spectra of the peptides K7W5 and R7W5 (225 to 229 nm) in the presence of *E. coli* liposomes.[20] The difference in the spectra of Os−C and Os−C(W_5) indicates that interactions between the tryptophan end-tag and the template sequence change the environment around the indole side chains and alter the CD signal. Clustering of tryptophan residues in the

https://doi.org/10.1021/acsomega.4c00478
ACS Omega 2024, 9, 15556−15572

sequence of Os−C(W_5) may hinder the accurate determination of the secondary structure.[25] Therefore, CD spectra of Os−C and Os−C(W_5) in SDS were further analyzed using K2D3. Os−C and Os−C(W_5) are predominantly disordered, with Os−C(W_5) having 13.5% more β-strand content (Table 1).

Table 1. Secondary Structure Analysis of Os−C and Os−C(W_5) in SDS

peptide	secondary structure constituent (%)		
	α-helix	β-strand	disordered
Os−C	0	19.3	81.7
Os−C(W_5)	0.6	32.8	66.6

Prinsloo et al. analyzed the spectra of Os−C using PSIPRED, a secondary structure prediction tool. In their analysis, the authors observed a β-strand content of 21%,[22] which is similar to the β-strand content of 19.3% obtained in this study. Overall, tryptophan end-tagging induces significant changes in the CD spectra in the presence of Tris buffer and SDS, especially between 220 and 230 nm.

Tryptophan End-Tagging Promotes Peptide Aggregation with Altered Membrane Penetration. MD simulations reveal that tryptophan end-tagging causes an increase in peptide aggregation and a change in membrane penetration, associated with minor but important changes in peptide conformation. Ramachandran plots of Os−C and Os−C(W_5) show that both peptides adopt a combination of a polyproline II and β-turn conformation centered around phi = −75° and psi = +150° (Figure 2A,B). Os−C(W_5) also adopts a β-sheet conformation centered around phi = −150° and psi = +150° (Figure 2B). Circular variance is a measure of the conformational flexibility of a peptide, and similarities in the circular variance of Os−C and Os−C(W_5) indicate that tryptophan end-tagging does not alter the conformational flexibility of Os−C (Figure 2C,D).

Snapshots of the simulation after 1 μs support the Ramachandran contour plot data and show that Os−C consists of segments with β-turns and disordered regions (Figure 2E), while Os−C(W_5) has the same segments as Os−C and in addition a β-bridge region (Figure 2F). β-bridges are short fragments that have similar binding patterns to β-sheet structures.[26] The presence of β-bridge regions in Figure 2F supports the presence of the β-sheet region in the Ramachandran plot of Os−C(W_5).

Simulations were also used to characterize hydrogen bond interactions between Os−C and Os−C(W_5) and the model *C. albicans* membrane. For Os−C, significant hydrogen bonding contributions are seen for Lys1, Arg4, Lys7, and Lys11 with some contributions from Tyr6, Tyr10, and Lys15 (Figure 3A). Tryptophan end-tagging does not affect hydrogen bonding by Lys1, Arg4, or Lys7, but while some hydrogen bonding by Lys15 and Lys18 is observed, hydrogen bond contributions from Tyr10 and Lys11 are substantially reduced (Figure 3B).

Tryptophan can form electrostatic, dipolar, hydrophobic, and hydrogen bond interactions with lipid headgroups and other molecules within the environment. The NH group in the indole side chain can serve as a hydrogen bond donor, while the aromatic ring can act as a hydrogen bond acceptor.[27] Of the five tryptophan residues, only Trp24 makes a substantial hydrogen bonding contribution, indicating that the other tryptophan residues could be involved in peptide aggregation.

Peptide penetration was measured by determining the depth of insertion of each residue. For both peptides, insertion occurs at approximately 100 ns and is initiated by residues at the N-terminus. Os−C residues interact with the membrane up to a depth of 0.25 nm up to Phe14, and minimal interaction is observed from Lys15 to Tyr19 (Figure 4A). By the end of the simulation, Tyr10 and Phe14 are inserted within the bilayer (Figure 4C).

For Os−C(W_5), insertion was restricted to the N-terminus, with six residues (Lys1 to Tyr6) inserted approximately 0.25 nm below the upper leaflet of the bilayer (Figure 4B). A snapshot of the simulation after 1 μs shows that Gly2, Ile3, and Arg4 were inserted into the upper leaflet of the bilayer (Figure 4D).

Manzo et al. observed for temporin B and pleurocidin that the initial insertion of AMPs into model Gram-negative and Gram-positive bacterial membranes proceeded via the N-terminus.[28,29] These studies showed that minor modifications to a peptide can fundamentally change the membrane interactions. Here, adding tryptophan residues to the C-terminus restricted membrane insertion by the N-terminal residues. Lack of insertion by tryptophan residues indicates that tryptophan residues may favor aggregation rather than membrane penetration.[30]

Self-association between peptides is critical and may either help or hinder activity.[31] Os−C forms transient aggregates but reverts to monomers for the majority of the simulation (Figure 5A). To investigate the interactions between individual peptides, an aggregation matrix was created. Contacts between Os−C peptides are mediated by Lys11 and Phe14 where the most membrane insertion occurs (Figure 5B). A snapshot of the simulation shows that the Os−C residues do not form close contacts, with one dimer formed at 850 ns showing Tyr19 (green) and Lys7 (blue) in close contact (Figure 5D, highlighted by the yellow oval).

Tryptophan end-tagging leads to the formation of a stable trimer throughout the simulation (Figure 5A) and increased contact between the residues. Interactions between the head (Lys1−Lys7) and tail regions (Tyr19−Trp24) and between tryptophan residues are present following end-tagging (Figure 5C). Furthermore, tryptophan residues mediate the aggregation of the peptide Os−C(W_5) (Figure 5E). Head-to-tail interactions do not affect membrane insertion (Figure 4A) of the head region (Lys1−Tyr6) and peptide-lipid hydrogen bonds mediated by Lys1 and Arg4 (Figure 3B). However, more interactions are mediated by residues 10−14 which insert into the membrane in the absence of the end-tag (Figure 5C). In the presence of the tryptophan end-tag, these residues do not insert into the membrane (Figure 4B), and Lys11 has a reduced hydrogen bond contribution (Figure 3B). These results show that tryptophan end-tagging enhances peptide aggregation, which inhibits membrane insertion and peptide-lipid hydrogen bonding.

Zai et al. modified the frog peptide temporin-PF (TPF) by removing Phe1 and replacing Phe9 and Phe13 with L- or D-enantiomers of tryptophan. Simulations performed in water indicated that TPF and its analogues formed dimers within 20 ns, and one of the tryptophan-containing analogues formed a stable tetramer. Similar to the results obtained in the present study, the addition of tryptophan resulted in stronger contacts between peptides, especially at the C-terminus.[30] Greater aggregation may lead to decreased antimicrobial activity since interpeptide interactions can prevent attachment to the cell

https://doi.org/10.1021/acsomega.4c00478
ACS Omega 2024, 9, 15556−15572

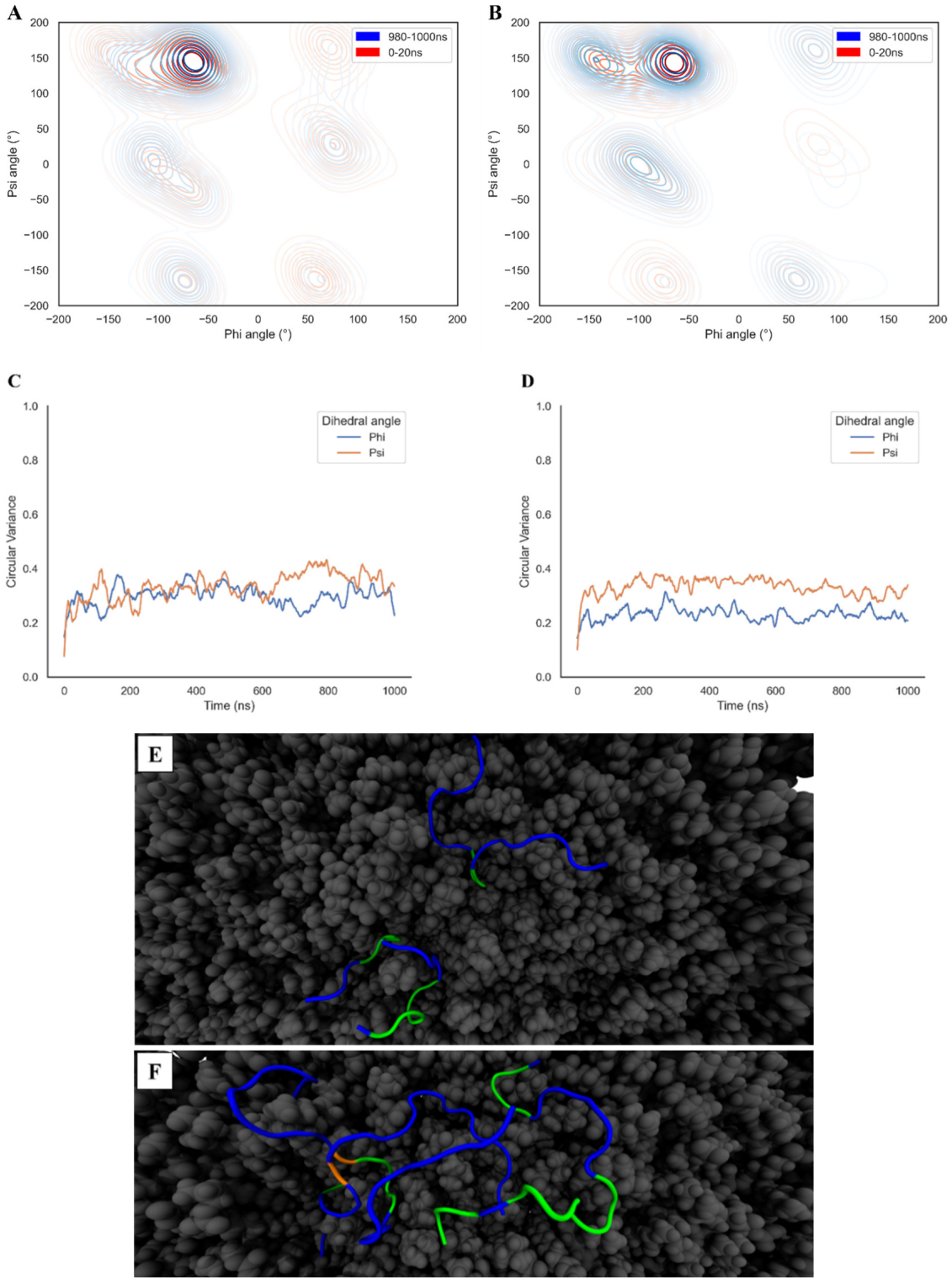

Figure 2. Secondary structure analysis of Os−C and Os−C(W_5). (A, B) Ramachandran contour plots were constructed for the first and last 20 ns of the simulation. (C, D) Circular variance of psi and phi angles for individual peptide residues were averaged for three peptides and plotted as a function of time. (E, F) Secondary structures of Os−C and Os−C(W_5) upon interaction with a *C. albicans* membrane after 1 μs. β-bridges are shown in orange, β-turns are shown in green, and coils are shown in blue. Images were created using Visual Molecular Dynamics (University of Illinois, Urbana−Champaign).

membrane and render the peptide inactive.[31] However, for some AMPs, aggregation is crucial for membrane permeabilization, disruption, and translocation.[32] MD simulations of melittin in a zwitterionic bilayer by Sengupta et al. showed that pore formation did not take place unless a cluster of at least three peptides was present.[33] Peptide activity is potentially enhanced due to a high localized concentration of peptide on the membrane surface prior to subsequent pore formation.[31] For membrane translocation, the peptides can aggregate before or during adsorption to the membrane surface and, if

https://doi.org/10.1021/acsomega.4c00478
ACS Omega 2024, 9, 15556−15572

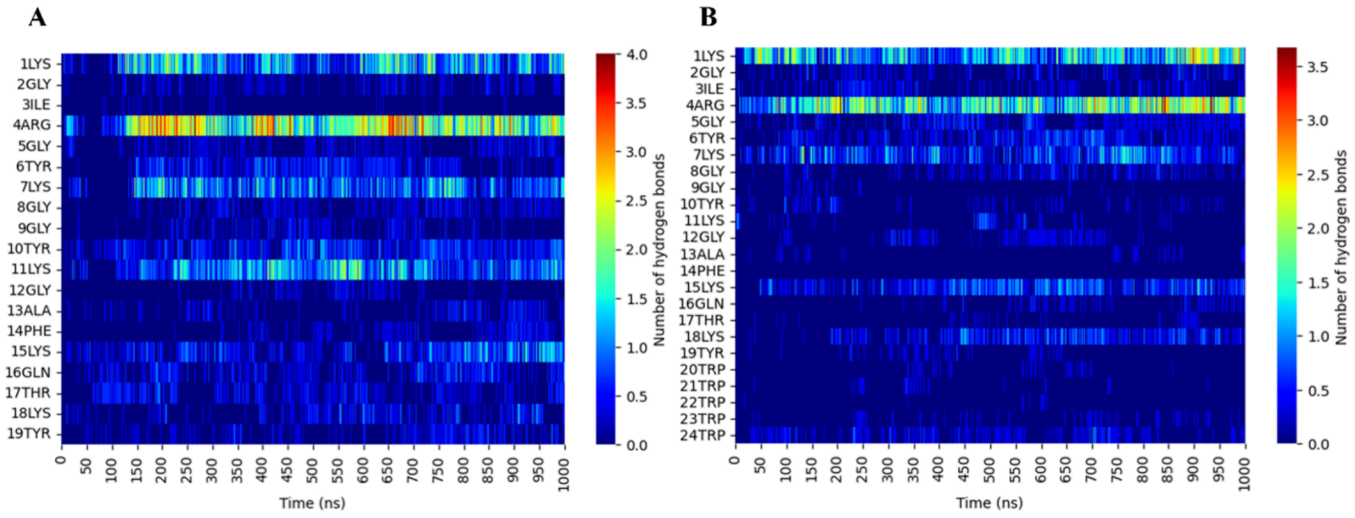

Figure 3. Hydrogen bonding between (A) Os−C and (B) Os−C(W_5) and the model membrane. Peptide-lipid hydrogen bonds are shown as a function of time for three peptides binding to a lipid bilayer.

hydrophobic enough, can cross the bilayer without inducing changes in permeability.[33]

Tryptophan End-Tagging Improves Anticandidal Activity. The antifungal activity of Os−C and Os−C(W_5) against planktonic and biofilm forms of *C. albicans* was investigated using microbroth dilution, biofilm prevention, and biofilm eradication assays. Tryptophan end−tagging, which doubles the hydrophobicity of Os−C (Materials and Methods, Table 4), leads to improved antifungal activity (Table 2 and Supplementary Figures 1−4).

No MIC and BIC_{50} values could be determined for Os−C, while an MIC of 50 μM and respective viability and biomass BIC_{50} values of 11.2 ± 3.69 and 10.6 ± 3.77 μM were determined for Os−C(W_5) (Table 2). Likewise, end-tagging GKH17 and HKH17 with tryptophan residues improves the antiplanktonic activity of the peptides against *C. albicans*.[17] Enhanced biofilm preventing activity is confirmed by inverted light microscopy images where treatment with 6.25 μM Os−C(W_5) or greater results in a decreased hyphal network, and aggregates of microcolonies are visible following treatment with 50 and 100 μM (Figure 6).

There are several studies on the effect of tryptophan end-tagging on the antiplanktonic activity of AMPs,[16−21] while to the best of our knowledge, no studies have investigated the effect of this modification on antibiofilm activity. Previously reported antifungal activity for GKH17 was determined in the presence of 0.01 M Tris buffer supplemented with 0.15 M NaCl to simulate a physiological environment. Tagging the peptide with five tryptophan residues led to improved activity in 0.15 M NaCl.[21] Previously, the antifungal activity of Os−C was determined in 0.01 M NaP buffer,[24] and although this study provided information on the mode of action of Os−C, further development for therapeutic applications was limited. With subsequent tryptophan end-tagging, Os−C has enhanced antiplanktonic and antibiofilm activities in a more complex RPMI-1640 medium that is considered physiologically relevant.

Os−C(W_5) Retains Some Antifungal Activity in Serum. Biofilms are clinically relevant and occur in physiological environments containing serum or plasma which often affects the activity of AMPs.[34] Therefore, the biofilm preventing activity of Os−C(W_5) was further evaluated in RPMI-1640 medium supplemented with 50% fetal bovine serum (FBS) (RPMI-1640-50% FBS). At 200 μM, approximately 20 times the BIC_{50}, Os−C(W_5) significantly reduces the *C. albicans* biofilm viability and biomass to 45.7 and 52.2%, respectively (Table 3). For biofilm eradication, 400 μM Os−C(W_5) is required to significantly reduce the viability of preformed biofilms to 82.4%; however, no significant reduction in biomass is observed (Table 3).

The data reveal that although reduced, Os−C(W_5) retains some antibiofilm activity in a serum-containing medium. Similar inhibitory effects of serum were reported by Sonesson et al. for 30 μM GHK17WWWWW against planktonic *C. parapsilosis* with approximately 50% less activity in the presence of 50% human serum than in physiological salt conditions.[21]

Tryptophan tagging of Os−C increases peptide activity in physiological salt solutions, such as RPMI-1640, but antibiofilm activity is reduced upon the addition of FBS. Given the complex composition of FBS, which contains proteins, carbohydrates, hormones, fatty acids, lipids, cytokines, inorganic compounds, vitamins, minerals, and growth factors,[35] it is probable that multiple components interfere with AMP activity. The instability in serum could be due to the binding of Os−C(W_5) to serum components such as albumin, proteolytic degradation by serum proteases, or the preferential binding of serum components to the fungal membrane which may prevent the peptide from interacting with the fungal membrane.[36] As a result, Os−C(W_5) will not interact with biofilm-associated cells, leading to diminished antibiofilm activity. Future strategies to overcome this limitation include noncovalent encapsulation of Os−C(W_5) into carrier molecules or conjugation of Os−C(W_5) to nanoparticles to limit nonspecific binding and/or the introduction of D-amino acids in the Os−C(W_5) sequence to increase resistance to proteases.[37]

Os-C(W_5) Retains Fungal Selectivity. For therapeutic purposes, AMPs must have a high selectivity for fungi, with limited toxicity toward host cells.[38] Using the hemolysis assay, the ability of Os−C(W_5) to induce erythrocyte hemolysis was investigated. Compared with the positive control (2% SDS) that caused significant hemolysis, Os−C(W_5) even at the highest concentration of 100 μM does not cause hemolysis and

https://doi.org/10.1021/acsomega.4c00478
ACS Omega 2024, 9, 15556−15572

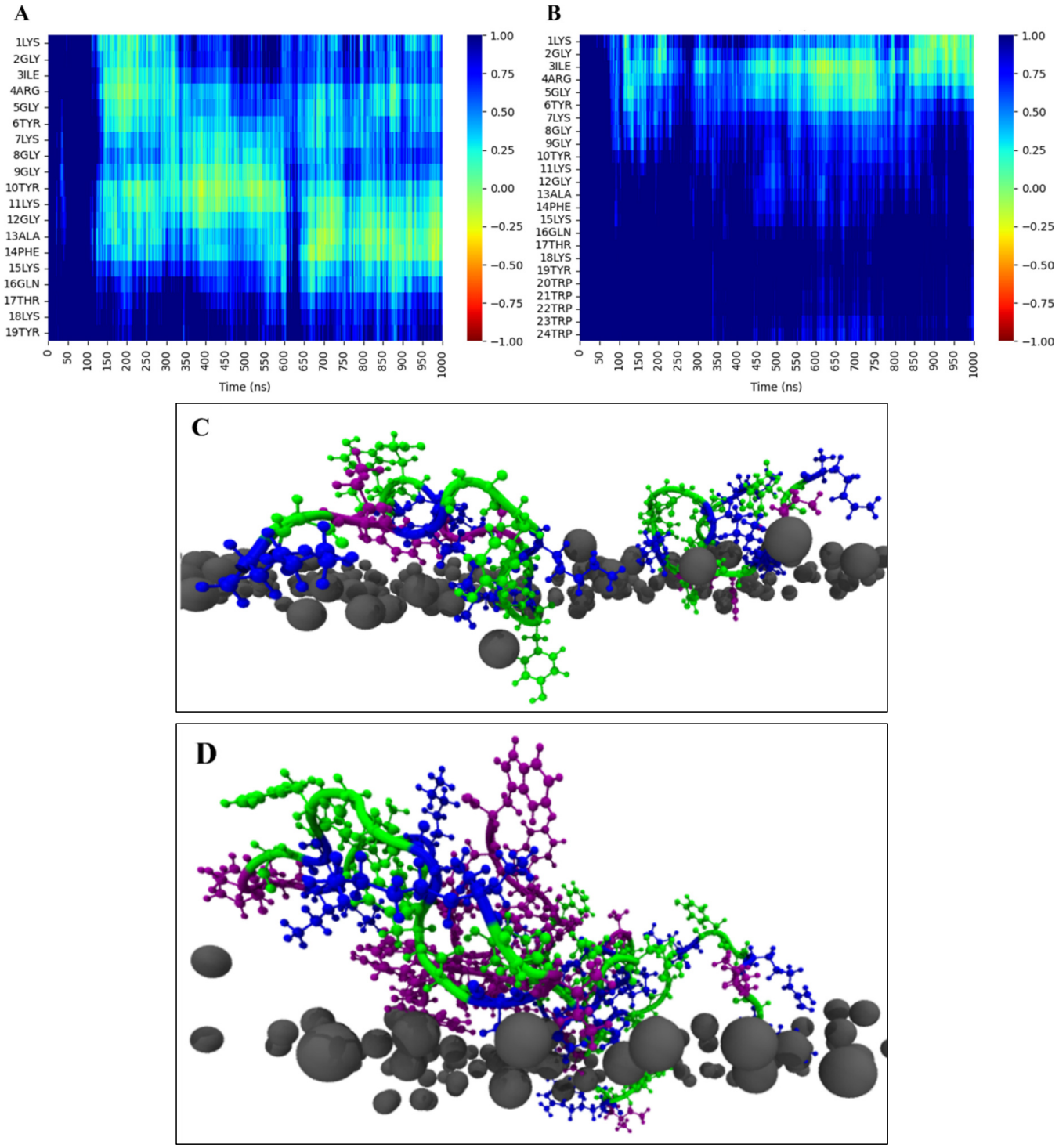

Figure 4. Insertion of Os−C and Os−C(W_5) into a *C. albicans* membrane. (A, B) Depth of insertion of the central carbon atom of each residue is calculated and averaged over all three peptides relative to the phosphate group plane in the upper leaflet of the bilayer. Positive and negative values indicate the peptides are above or below the phosphate group of the upper leaflet of the bilayer, respectively. (C, D) Basic residues are blue, nonpolar residues are purple, polar residues are green, and gray spheres represent the phosphorus atom in the phosphate headgroup of the lipids in the upper leaflet of the bilayer. Images were designed using Visual Molecular Dynamics (University of Illinois at Urbana−Champaign).

differences are not significant when compared with the untreated control (Figure 7).

Likewise, in a previous study, Os−C at 100 μM did not cause hemolysis, indicating that tryptophan end-tagging of Os−C at the C-terminal did not increase cytotoxicity.[22] Pasupuleti et al. reported low levels of hemolysis of 6 and 10% for 60 μM of tagged KNK-7-WWWWW, and KNK-10-WWWWW respectively, although compared with the respective nontagged peptides, differences in hemolysis were significant.[16]

Antiplanktonic Activity of Os−C(W_5) Is due to ROS Formation and Not Increased Membrane Permeability. For further mode of action studies of Os−C(W_5), the number of cells used was increased from 1.5×10^5 to 2.5×10^6 CFU/

https://doi.org/10.1021/acsomega.4c00478
ACS Omega 2024, 9, 15556−15572

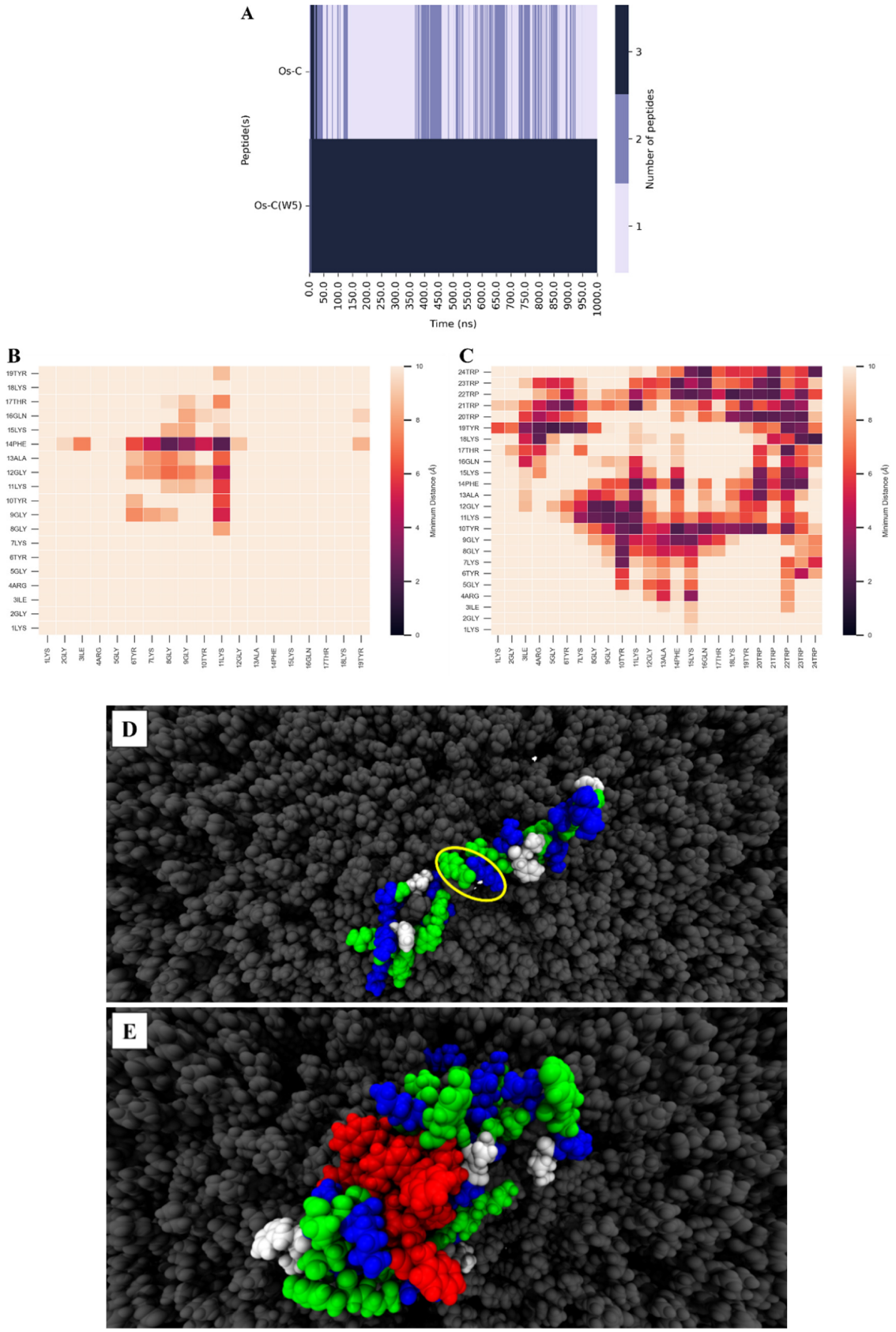

Figure 5. Tryptophan end-tagging promotes peptide aggregation. (A) Formation of peptide oligomers was recorded for the duration of the simulation. (B, C) Average distances between (B) Os−C and (C) Os−C(W_5) residues. (D) Dimer formation by Os−C after 850 ns. (E) Trimer formation by Os−C(W_5) after 1 μs. For (D) and (E), basic residues are blue, nonpolar residues are white, and polar residues are green. Aggregation caused by tryptophan residues is shown in red. The yellow oval highlights the interaction between Tyr19 (green) and Lys7 (blue). Images were designed using Visual Molecular Dynamics (University of Illinois at Urbana−Champaign).

https://doi.org/10.1021/acsomega.4c00478
ACS Omega 2024, 9, 15556−15572

Table 2. Antifungal Activity of Amphotericin B, Os−C, and Os−C(W_5)

	MIC[a] (μM)	BIC_{50}[b] (μM)		BEC_{50}[c] (μM)	
		viability	biomass	viability	biomass
amphotericin B	0.625	0.06 ± 0.01	0.05 ± 0.02	0.08 ± 0.00	0.56 ± 0.20
Os−C	>100	>100	>100	ND[d]	ND
Os−C(W_5)	50	11.2 ± 3.69	10.6 ± 3.77	69.3 ± 11.3	87.4 ± 11.8

[a]Lowest concentration of antifungal that reduced planktonic cell growth by ≥90%. [b]Lowest concentration of antifungal that caused a 50% reduction in biofilm cell viability or biomass. [c]Lowest concentration of antifungal that reduced the viability or biomass of a preformed biofilm by 50%. [d]ND, not determined. All data represents the mean ± SEM of three independent experiments.

mL to enable the direct comparison of results, irrespective of the assay used. Isopropanol, the positive control for membrane permeabilization, significantly reduces cell viability to 1.3%, while 0.312 and 0.625 μM amphotericin B (AMB) significantly reduces cell viability to 38 ± 10.4 and 26 ± 6.6%, respectively (Figure 8). For 3.12−50 μM Os−C(W_5), a dosage-dependent decrease in viability is observed from 73 ± 2.1 to 4.3 ± 4.3% compared with the untreated control. A similar effect was reported by D'Auria et al., who evaluated the effect of the peptide temporin G on *C. albicans* viability using methylene blue dye.[39]

Antifungal peptides are known to kill cells by using multiple modes of action including membrane permeabilization, ROS production, ATP efflux, cell cycle impairment, disrupted cation homeostasis, cell autophagy, and abnormal vacuole function.[40] Previously, we showed that the parent peptide, Os, causes membrane permeabilization, while the derivative Os−C induces ROS production.[24] Using the same conditions and concentrations used for cell viability, cell permeability was determined with the SYTOX Green assay. Isopropanol increased the membrane permeability, while AMB and Os−C(W_5) have no membrane-permeabilizing activity at any of the relevant concentrations (Figure 9).

Tryptophan end-tagging has been identified as an AMP modification that promotes membrane permeabilization.[16−20] In contrast, a novel finding in the present study is that tryptophan end-tagging does not cause membrane permeabilization but rather ROS production, further supported by MD simulations where minimal membrane insertion is observed for Os−C(W_5) (Figure 4B).

In a study by Bellavita et al., the mode of action of several cyclic temporin L isoforms was not liposome leakage but rather membrane surface aggregation as the incubation of *C. albicans* cells with these antifungal peptides caused a decrease in the zeta potential. This mode of action was further evaluated using liposomes with thioflavin T (ThT) as a probe, and the effects on liposome topography were evaluated with atomic force microscopy. The authors hypothesized that aggregation led to a carpeting effect, but the consequence on cellular function was not identified.[41] Likewise, to further support the initial MD simulation findings in the present study, in vitro based studies can be undertaken to determine the effect of aggregation on the zeta potential of *C. albicans* cells, further supported by ThT fluorescence studies. Due to the higher resolution of field electron scanning electron microscopy, this technique can be used to identify the aggregates and to determine the effect on liposome membranes.[42]

For several AMPs, including Os−C, ROS production plays a key role in the antifungal activity[43,44] and subsequent mitochondrial damage,[45] membrane lipid oxidation,[46] and formation of advanced glycation protein products[47] that contribute to cell death via apoptosis or necrosis. Using the 2′,7′-dichlorodihydrofluorescin diacetate (DCFH-DA) assay, for 25 μM of Os−C(W_5), there is a time-dependent increase in ROS production (Figure 10A). A dosage effect in ROS production is observed in the absence of 10 mM ascorbic acid, which is significantly increased for 12.5 and 25 μM Os−C(W_5) after 3 h (Figure 10B). To confirm that increased ROS production is linked to the antifungal activity of Os−C(W_5) resulting in cell death, cell viability was evaluated in the presence and absence of 10 mM ascorbic acid. A significant increase in cell viability in the presence of ascorbic acid and Os−C(W_5) is observed indicating that ascorbic acid protects *C. albicans* from the antifungal ROS-mediated activity of Os−C(W_5) (Figure 10C). Similar findings were reported in a recent study on the peptide AMP-17 derived from the domestic housefly *Musca domestica* where the MIC of the peptide against *C. albicans* increased from 20 to 40 μg/mL in the presence of 5 mM ascorbic acid and increased from 20 to 160 μg/mL in the presence of 50 mM ascorbic acid.[48]

The present study shows that tryptophan end-tagging of the peptide Os−C does not alter the mode of action as the antifungal activity of Os−C(W_5) is also linked to ROS production. Peptides such as HsAFP1[49,50] and NaD1[51,52] are known to enter fungal cells and induce ROS production. Thevissen et al. observed that the plant defensin RsAFP2 does not enter the cell but interacts with the glycosphingolipid glucosylceramide and induces membrane permeabilization, ROS production, cell wall stress, septin mislocalization, and metacaspase-independent apoptosis.[53]

For Os−C(W_5), MD simulations reveal that Os−C(W_5) has reduced peptide-membrane interactions and insertion into a *C.*

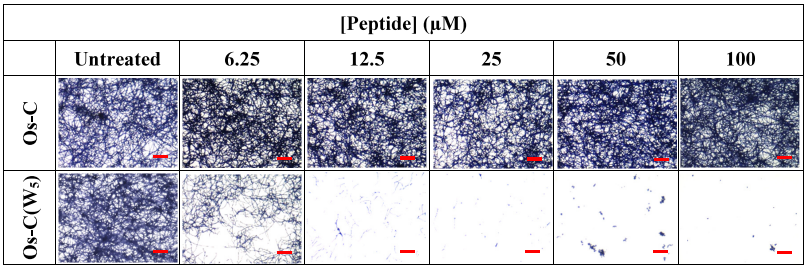

Figure 6. Biofilm preventing activity of Os−C(W_5). Biofilms were grown in the presence of Os−C or Os−C(W_5) for 24 h and then stained with 0.1% crystal violet. Images are representative of three independent experiments and taken at 10× magnification. Scale bar = 100 μm.

https://doi.org/10.1021/acsomega.4c00478
ACS Omega 2024, 9, 15556−15572

Table 3. Antibiofilm Activity of Ampotericin B (AMB) and Os−C(W_5) in FBS[a]

	biofilm prevention		biofilm eradication	
	viability (%)	biomass (%)	viability (%)	biomass (%)
2.5 μM AMB	0.40 ± 0.10****	0.92 ± 0.49****	21.2 ± 0.81****	55.7 ± 15.1*
200 μM Os−C(W_5)	45.7 ± 6.24****	52.2 ± 3.91****	ND[b]	ND
400 μM Os−C(W_5)	ND	ND	82.4 ± 1.41****	95.5 ± 2.97

[a]Data represent mean ± SEM (n = 3). One-way ANOVA was performed followed by a posthoc Dunnett's multiple comparisons test. Asterisks (*p < 0.05; ****p < 0.0001) represent a significant difference compared with the untreated control which represents 100% viability or biomass. [b]ND, not determined.

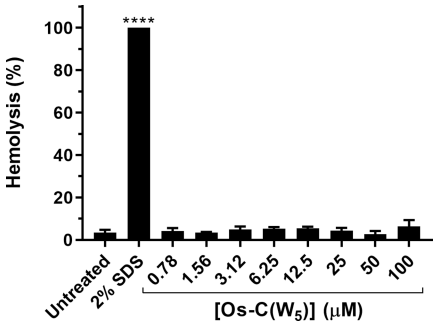

Figure 7. Hemolytic activity of Os−C(W_5). Human erythrocytes were exposed to Os−C(W_5) (0.78−100 μM) for 30 min and then absorbance was measured at 570 nm. SDS (2%) was used as a positive control. Data represent the mean ± SEM (n = 3). One-way ANOVA was performed followed by a posthoc Dunnett's multiple comparisons test. Asterisks (****p < 0.001) represent a significant difference compared with the untreated control.

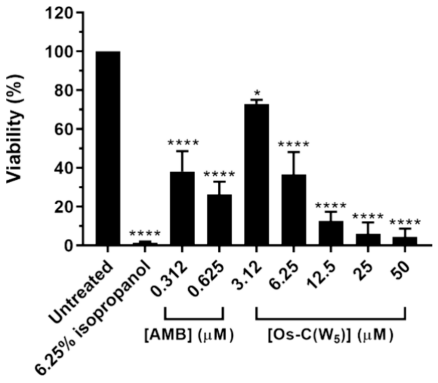

Figure 8. Effect of AMB and Os−C(W_5) on planktonic cell viability. *C. albicans* cells (2.5 × 10^6 CFU/mL) were incubated with isopropanol (6.25%), AMB (0.312−0.625 μM), and Os−C(W_5) (3.12−50 μM) for 3 h, and cell viability was quantified using CellTiter Blue. Data represent the mean ± SEM (n = 3). One-way ANOVA was performed followed by a posthoc Dunnett's multiple comparisons test. Asterisks (*p < 0.05; ****p < 0.001) represent a significant difference compared with the untreated control.

albicans membrane and enhanced peptide aggregation. Although MD simulations provide important information on how AMPs induce pore formation, findings showing reduced membrane interaction allude to alternative mechanisms associated with AMP-mediated growth inhibition or cell death. The cell wall of *C. albicans*, besides containing polysaccharide components, also contains many proteins involved in adhesion, hyphal development, and biofilm formation such as enzymes, morphology-associated proteins, adhesins, and binding (receptor) proteins. Disruption of the cell wall integrity and/or protein function leads to oxidative

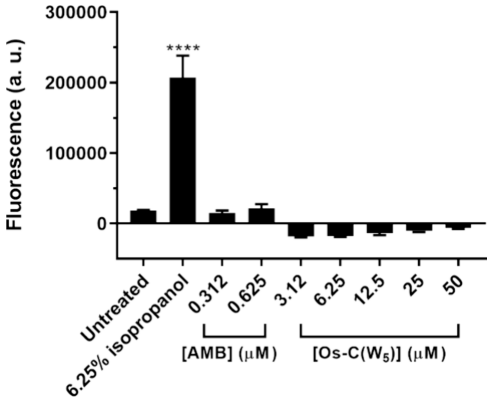

Figure 9. Membrane-permeabilizing activity of AMB and Os−C(W_5). *C. albicans* cells (2.5 × 10^6 CFU/mL) were exposed to isopropanol (6.25%), AMB (0.312−0.625 μM), and Os−C(W_5) (3.12−50 μM) in the presence of SYTOX Green, and fluorescence was measured after 3 h. Data represent the mean ± SEM (n = 3). One-way ANOVA was performed followed by a posthoc Dunnett's multiple comparisons test. Asterisks (****p < 0.001) represent a significant difference compared with the untreated control.

stress and associated ROS formation and, when in excess, inhibits the cell wall integrity pathway leading to growth inhibition or cell death.[54] Interestingly, for both Os−C and Os−C(W_5), ROS formation is the identified mode of action, and although MD simulations clearly show differences in membrane insertion, the production of ROS is associated with residues in the Os−C sequence rather than the presence of terminal tryptophan residues or a change in the secondary structure of the peptide. It would also be interesting to ascertain if Os−C(W_5) aggregation leads to increased ROS production when compared with Os−C. Therefore, further studies should focus on the interaction with other cell wall components as well as the identification of key amino acids or sequences associated with ROS production.

Os−C(W_5) Induces Morphological Changes. ROS-mediated oxidative stress in *Candida* species causes cellular dysfunction and associated changes to morphology that can be evaluated with scanning electron microscopy.[55] Untreated cells are oval-shaped, with a smooth surface and an intact cell wall with cell buds and bud scars (Figure 11A). Treatment with 6.25 μM Os−C(W_5) induces cell rounding, surface roughness, bleb formation (Figure 10B, arrowheads), and leakage of intracellular content (Figure 11B, thick arrow). At 12.5 μM Os−C(W_5) (Figure 11C), these effects are more pronounced, and in addition, cracks on the cell surface (Figure 11C, chevrons) and the presence of cellular debris (Figure 11C, star) are observed.

Increased surface roughness, blebbing, and leakage of cytoplasmic content are commonly seen after treatment with

https://doi.org/10.1021/acsomega.4c00478
ACS Omega 2024, 9, 15556−15572

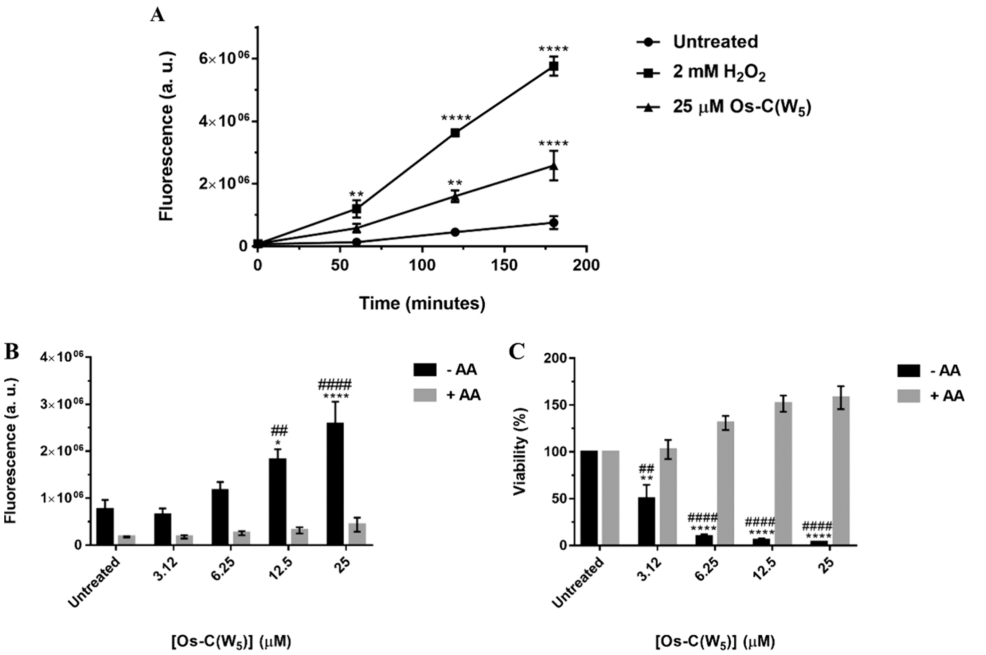

Figure 10. ROS production by Os−C(W_5). (A) Cells (2.5 × 10^6 CFU/mL) were treated with 25 μM Os−C(W_5). Then, fluorescence was measured every hour for 3 h. Hydrogen peroxide (2 mM) was used as a positive control. Data represent the mean ± SEM (n = 3). One-way ANOVA was performed followed by a posthoc Dunnett's multiple comparisons test. Asterisks (**p < 0.01; ****p < 0.0001) represent a significant difference compared with the untreated control. (B) ROS production in the presence and absence of 10 mM ascorbic acid was measured after 3 h. Data represent the mean ± SEM (n = 3). (C) Cell viability in the presence and absence of 10 mM ascorbic acid was measured after 3 h. Data represent the mean ± SEM (n = 3). For (B) and (C), two-way ANOVA was performed followed by a posthoc Tukey's multiple comparisons test. Asterisks (*p < 0.05; **p < 0.01 ****p < 0.0001) represent a significant difference compared with the untreated control, and hash symbols ($^{\#\#}p$ < 0.01; $^{\#\#\#\#}p$ < 0.0001) represent a significant difference in fluorescence in the presence and absence of 10 mM ascorbic acid.

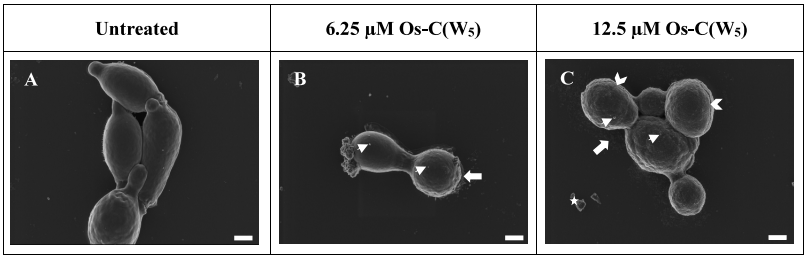

Figure 11. Effect of Os−C(W_5) on the morphology of planktonic *C. albicans*. Cells (2.5 × 10^6 CFU/mL) were (A) untreated or treated with (B) 6.25 μM or (C) 12.5 μM Os−C(W_5) for 3 h; then, samples were prepared and viewed using scanning electron microscopy. Effects on cells include extracellular debris (star), leakage of intracellular content (thick arrows), blebs (arrowheads), and cracking (chevrons). Images were taken at 20,000× magnification. Scale bar: 1 μm.

antifungal agents and are indicators of membrane damage.[56,57] Since Os−C(W_5) does not permeabilize the membrane, the observed cellular damage is likely the consequence of excessive ROS formation which may damage the membrane by oxidizing membrane-associated lipids and proteins.

Os−C(W_5) Inhibits Biofilm Formation by Reducing Adhesion and Extracellular Matrix Production. Biofilm formation occurs in four sequential steps: adhesion, initiation, maturation, and dispersal.[58] To further investigate the effect of Os−C(W_5) on this process, the effect of Os−C(W_5) on critical events such as adhesion and ECM production was investigated. Inhibition of adhesion by Os−C(W_5) was investigated, and a significant decrease in adhesion of about 20% is observed for both 0.078 μM AMB and 10 μM Os−C(W_5) (Figure 12).

Exposure to 3, 10, and 64 μM LL-37 for 30 min reduced *C. albicans* adhesion to polystyrene and silicone surfaces by 35, 59, and 80%, respectively.[59,60] Likewise, 1 μM psoriasin reduced the adhesion of *C. albicans* to polystyrene by 20% within 30 min.[61] Likewise, 10 μM of Os−C(W_5) causes a decrease in cell adhesion that is less than LL-37 but greater than psoriasin, indicating that reduced adhesion contributes to the prevention of biofilm formation.

The ECM serves as a protective barrier for cells within the biofilm.[9] Direct cell killing or inhibition of the ECM synthesis pathways can prevent ECM formation. In this study, the amount of carbohydrates, proteins, and nucleic acids in the ECM following exposure to AMB and Os−C(W_5) was quantified using several biochemical analyses. This approach to quantifying individual ECM components has been applied to phytoactive compounds[62] and the antifungal drug fluconazole[63] and serves as an initial indicator of the pathways involved.

Carbohydrates are less abundant and make up approximately 25% of the *C. albicans* ECM and represent the most complex fraction of the matrix. Monosaccharides such as glucose, xylose, mannose, and arabinose are present in the highest

https://doi.org/10.1021/acsomega.4c00478
ACS Omega 2024, 9, 15556−15572

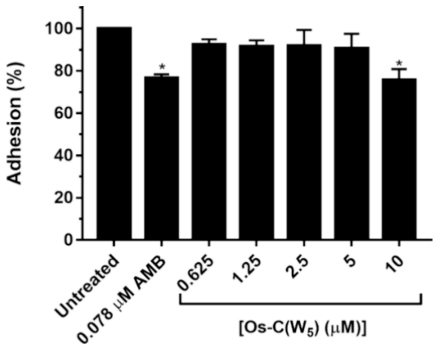

Figure 12. Effect of Os−C(W_5) on *C. albicans* adhesion. *C. albicans* (1×10^6 CFU/mL) was incubated in the presence of 0.078 μM AMB or Os−C(W_5) (0.625−10 μM) for 1 h; then, adhesion was quantified by solubilizing bound crystal violet with 30% acetic acid and then measuring the absorbance. Data represent the mean ± SEM (n = 3). One-way ANOVA was performed followed by a posthoc Dunnett's multiple comparisons test. Asterisks (*p < 0.05) represent a significant difference compared with the untreated control.

quantities.[64] A significant reduction in carbohydrate content is observed at the two highest concentrations of AMB (Figure 13A) and Os−C(W_5) (Figure 13D) with the absence of carbohydrates at 10 μM Os−C(W_5). The most abundant ECM components are proteins which account for 55% of the dry weight of *C. albicans* ECM.[9] Exposure to AMB and Os−C(W_5) leads to a significant decrease of protein associated with the ECM at 0.039−0.156 μM AMB (Figure 13B) and 2.5−10 μM Os−C(W_5) (Figure 13E). Extracellular nucleic acids are the least abundant and comprise 5% of the ECM, maintaining the structural integrity of the biofilm and playing an additional role in linking matrix components.[65] A significant decrease in biofilm-associated nucleic acids is observed for 0.078 and 0.156 μM AMB (Figure 13C) and 2.5−10 μM Os−C(W_5) (Figure 13F).

CONCLUSIONS

Inactivity of AMPs in physiological salt environments, serum, and plasma often limits further therapeutic development. Tryptophan end-tagging of Os−C, an inactive peptide, leads to enhanced antifungal activity against *C. albicans*. In silico and steady-state analyses using MD simulations and CD demonstrate that this modification alters the secondary structure of Os−C. Furthermore, MD simulations show that end-tagging leads to reduced membrane insertion and enhanced peptide aggregation which is corroborated by a lack of membrane permeabilization and hemolysis in vitro. Instead of membrane permeabilization, the induction of ROS is linked to the antifungal activity of Os−C(W_5) and leads to reduced cell viability and morphological changes. The antibiofilm activity of Os−C(W_5) is characterized by reduced cell adhesion and viability, which leads to reduced ECM production. Finally, although reduced, antibiofilm activity is retained in a serum-containing medium. Tryptophan end-tagging is a viable strategy for improving the antifungal activity of Os−C against *C. albicans* in a physiologically relevant salt environment.

MATERIALS AND METHODS

Antifungal Agents. All peptides (Table 4) were purchased from GenScript (Piscataway, New Jersey, USA). The purity (>95%) and molecular mass of the peptides Os−C and Os−C(W_5) were determined by the vendor using reverse-phase HPLC and mass spectrometry, respectively (Supplementary

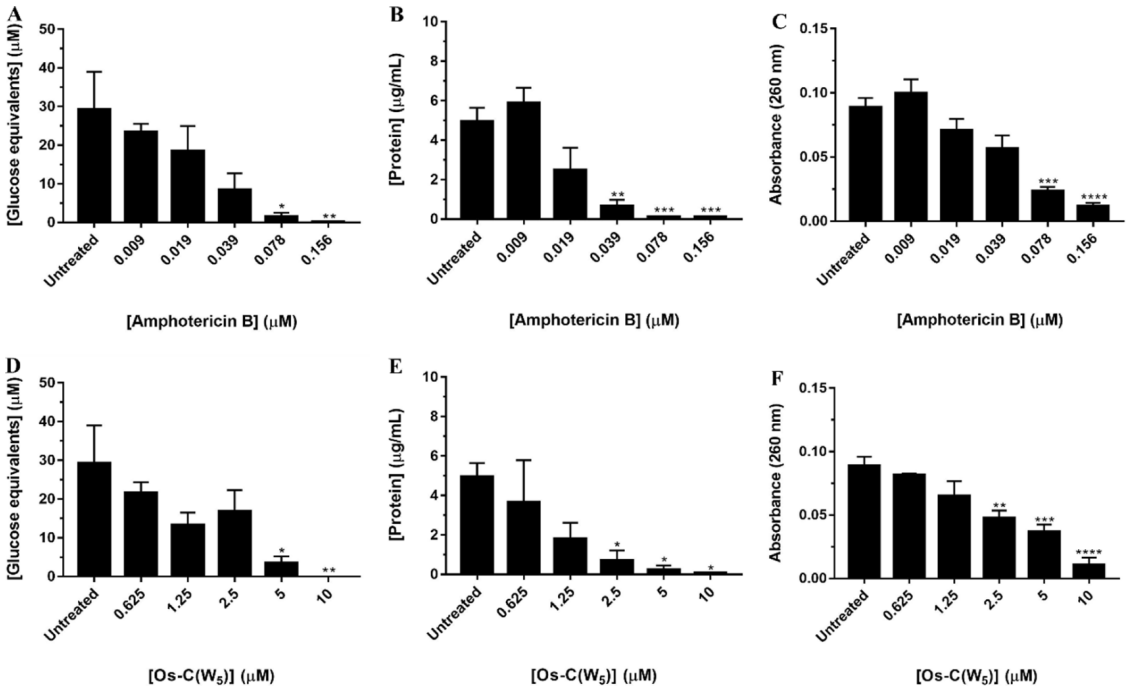

Figure 13. Effect of (A−C) AMB and (D−F) Os−C(W_5) on the formation of carbohydrates, proteins, and nucleic acids in the ECM of *C. albicans* biofilms. Cells (1×10^6 CFU/mL) were exposed to AMB (0.009−0.156 μM) and Os−C(W_5) (0.625−10 μM) for 24 h; then, soluble ECM was extracted from treated and untreated samples. Carbohydrates, proteins, and nucleic acids were quantified. Data represent the mean ± SEM of three independent experiments. One-way ANOVA was performed followed by a posthoc Dunnett's multiple comparisons test. Asterisks (*p < 0.05; **p < 0.01; ***p < 0.001) represent a significant difference compared with the untreated control.

https://doi.org/10.1021/acsomega.4c00478
ACS Omega 2024, 9, 15556−15572

Table 4. Physicochemical Properties of Peptides Used in the Study

peptide	sequence	molecular weight[a] (g/mol)	charge[a]	pI[a]	hydrophobicity[b] (%)
Os−C	KGIRGYKGGYKGAFKQTKY	2150.49	+6	10.8	15.8
Os−C(W_5)	KGIRGYKGGYKGAFKQTKY**WWWWW**	3081.55	+6	10.8	33.3

[a]Calculated using GenScript peptide-molecular-weight-calculator (https://www.genscript.com/tools/peptide-molecular-weight-calculator). [b]Calculated using peptide 2.0 (https://www.peptide2.com/N_peptide_hydrophobicity_hydrophilicity.php).

Figures 5−8). The peptide concentration was determined using the formula:

$$c = \frac{A_{280} \times \mathrm{df} \times \mathrm{MW}}{n_{\mathrm{Tyr}}(\varepsilon_{\mathrm{Tyr}}) + n_{\mathrm{Trp}}(\varepsilon_{\mathrm{Trp}})}$$

where c is the concentration in mg/mL, A_{280} is the absorbance at 280 nm, df is the dilution factor, MW is the molecular weight in mg/mmol, and $n_{\mathrm{Tyr/Trp}}(E_{\mathrm{TYR}}/E_{\mathrm{TRP}})$ is the number of tyrosine or tryptophan residues and their corresponding extinction coefficients (tyrosine = 1200 AU/mmol/mL; tryptophan = 5560 AU/mmol/mL). Once the peptide concentration was determined, stocks were prepared in double-distilled water (ddH_2O), and aliquots were stored at −20 °C. AMB (Sigma-Aldrich, St Louis, Missouri, USA) was used as the control drug, and stocks were prepared in dimethyl sulfoxide (DMSO; Sigma-Aldrich, St Louis, Missouri, USA) and then stored at −80 °C.

Secondary Structure Analysis. The secondary structure of the peptides was analyzed using CD spectroscopy. Os−C and Os−C(W_5) (both 50 μM) were dissolved in 5 mM Tris (Sigma-Aldrich; St Louis, Missouri, USA) or 50 mM SDS (Sigma-Aldrich, St Louis, Missouri, USA). Spectra were obtained using a J-1500 CD spectrophotometer (Jasco; Easton, Maryland, USA). Scans were performed at 20 °C over the 180−260 nm range, with a path length of 0.2 cm, a scan speed of 100 nm/min, a data pitch of 0.5 nm, and a bandwidth of 2 nm. High-tension voltage values above 600 V were excluded. Samples were scanned ten times and then corrected for solvent effects. The CD spectra of Os−C and Os−C(W_5) were further analyzed using K2D3, an online secondary structure estimation tool.[66]

Molecular Dynamics Simulations. Simulations were carried out using GROMACS.[67] The CHARMM36m all-atom force-field was used in all simulations,[68,69] and the initial bilayer configuration was designed in a water box measuring 90 × 90 × 110 nm using CHARMM-GUI.[70] Membranes contained 256 lipids composed of 1-palmitoyl-2-oleoyl-*sn*-glycero-3-phosphocholine, 1-palmitoyl-2-oleoyl-*sn*-glycero-3-phosphoethanolamine, 1-palmitoyl-2-oleoyl-*sn*-glycero-3-phospho-L-serine, 1-palmitoyl-2-oleoyl-*sn*-glycero-3-phosphoinositol, and ergosterol (in a 59:21:3:4:13 ratio) to reflect the composition of the *C. albicans* membrane.[71,72]

Peptides were designed using Avogadro software, and then the starting structures were obtained by running a simulation of the peptides in water for 1 ns. In order to investigate the collective behavior of these AMPs, three peptides were inserted 9.7 Å above the lipid bilayer in random positions and orientations at least 5 Å apart from each other to identify possible peptide−peptide interactions. The system was solvated with TIP3P water and neutralized by sodium and chloride ions. Energy minimization was carried out using the steepest descent algorithm until the maximum force was less than 1000 kJ/mL/nm. Equilibration was run using the NVT ensemble for 250 ps with a target temperature of 310 K and then the NPT ensemble for 1625 ps with a target temperature and pressure of 310 K and 1 bar, respectively, with position restraints on the peptides at a temperature of 310 K and a pressure of 1 bar. Production simulations were run for 1 μs using a semi-isotropic NPT ensemble using 2 fs timesteps. All production simulations were performed at a temperature of 310 K which was controlled by a Nose-Hoover thermostat and a pressure of 1 bar, which was controlled by a Parrinello−Rahman barostat.

The conformation of the peptides was quantified by measuring torsion angles, which are circular quantities, and the circular mean of psi or phi angles was calculated as follows:

$$\bar{\psi} = \mathrm{atan2}\left(\frac{1}{n}\sum_{j=1}^{n}\sin\psi_j, \frac{1}{n}\sum_{j=1}^{n}\cos\psi_j\right)$$

Circular variance is calculated as the spread of angles across all peptides and timesteps for each residue and was determined using the equation:

$$\mathrm{Var}(\psi) = 1 - R_{\mathrm{av}}$$

with R being given by

$$R^2 = \left(\sum_{i=1}^{n}\cos\psi_i\right)^2 + \left(\sum_{i=1}^{n}\sin\psi_i\right)^2$$

The average psi and phi dihedral angles were used to create a Ramachandran contour plot, with contours representing all the dihedral angles for the first and last 20 ns of the simulation.

Hydrogen bond analysis measured the number of hydrogen bonds formed between all hydrogen bond donors and acceptors between each residue and membrane lipids. The distance and angle cutoff values for identifying hydrogen bonds were 3 Å and 150°, respectively. Peptide insertion into the lipid bilayer was determined by the z-position analysis which measured the z-position of the central carbon atom of each residue relative to the average z-position of the phosphate group plane in the upper leaflet of the lipid bilayer. A negative value indicated the insertion of a residue into the membrane. Peptide aggregation was evaluated by a cluster analysis, which measured the number of peptide oligomers formed during the simulation, and an aggregation matrix, which investigated interactions between individual residues. If the peptides were within 6 Å of each other, they were considered to be in the same oligomer.

Antiplanktonic Activity. *C. albicans* ATCC 90028 cells were obtained from the American Type Culture Collection (Manassas, Virginia, USA). Cells were prepared as described in the EUCAST Definitive Document EDef 7.1.[73] Briefly, cells were streaked on a yeast peptone dextrose (YPD) agar plate and incubated for 18−24 h at 37 °C. Single colonies were suspended in ddH_2O and then diluted in ddH_2O to the required cell density. For all antifungal assays, for the AMB and relevant controls, the final DMSO concentration was 0.5%.

https://doi.org/10.1021/acsomega.4c00478
ACS Omega 2024, 9, 15556−15572

Antiplanktonic activity was determined according to the EUCAST Definitive Document EDef 7.1.[73] AMB (0.009−2.5 μM) and Os−C and Os−C(W_5) (0.78−200 μM) were prepared in double-strength RPMI-1640 supplemented with 2% glucose (2× RPMI-1640-2% G). A 50 μL aliquot of each antifungal was added to a 96-well polypropylene plate (Greiner Bio-One; Kremsmünster, Austria). Then, 50 μL of *C. albicans* cells suspended in ddH_2O at a density of 3×10^5 CFU/mL was added. The final concentration range of AMB was 0.004−1.25 μM and that of Os−C and Os−C(W_5) was 0.39−100 μM. Following 24 h incubation at 37 °C, cell growth was determined by measuring the optical density at 530 nm. The MIC was defined as the lowest concentration of antifungal that inhibited fungal growth by at least 90%.[73]

For the mode of action studies, the effect of AMB and Os−C(W_5) on the metabolic activity of planktonic cells was determined using the CellTiter Blue (CTB, Promega, Madison, Wisconsin, USA) cell viability assay. AMB (0.625 and 1.25 μM) and 6.25−100 μM of Os−C(W_5) in a volume of 50 μL were added to the wells of a 96-well polypropylene plate. Then, 50 μL of a cell suspension, at a cell density of 5×10^6 CFU/mL, was added to AMB or Os−C(W_5). The final concentrations of AMB and Os−C(W_5) were 0.312−0.625 μM and 3.12−50 μM, respectively. After 3 h incubation, the cell viability was determined by adding CTB (11 μL) to each well, and after 1 h at 37 °C incubation in the dark, the fluorescence was measured at an excitation wavelength (Ex) of 535 nm and emission wavelength (Em) of 590 nm.

Antibiofilm Activity. For both the biofilm prevention (including mode of action studies) and eradication studies, single colonies were placed in YPD broth and incubated for 18 h at 30 °C. The overnight culture was centrifuged, the supernatant was discarded, and the pellet was washed and resuspended in RPMI-1640 to a cell density of 2×10^6 CFU/mL for biofilm prevention, adhesion, and ECM analysis assays. For biofilm eradication assays, the cell density was adjusted to 1×10^6 CFU/mL.

Biofilm preventing activity was investigated by adding 50 μL of the cell suspension as described above (2×10^6 CFU/mL) to 50 μL of AMB (0.019−5 μM), Os−C, or Os−C(W_5) (both 0.78−200 μM) in the wells of a sterile, 96-well polystyrene plate (Greiner Bio-One; Kremsmünster, Austria). The final concentration range of AMB was 0.004−2.5 μM and those of Os−C and Os−C(W_5) was 0.39−100 μM. Cells were incubated for 24 h at 37 °C without shaking; then, the medium was removed, and cells were washed with 100 μL of PBS.

To determine activity against preformed biofilms, 100 μL of the cell suspension (1×10^6 CFU/mL) was added to the wells of a sterile, 96-well polystyrene plate and then incubated for 24 h at 37 °C without shaking. After 24 h, the biofilms were washed with 100 μL of PBS, and then, 100 μL of AMB (0.009−2.5 μM) or Os−C(W_5) (0.39−100 μM) was added followed by further incubation for 24 h at 37 °C without shaking. The medium was then removed, and the biofilm was washed with 100 μL of PBS.

Biofilm preventing and eradicating activity of Os−C(W_5) in serum was then further investigated in RPMI-1640−50% FBS. For biofilm prevention, to a cell suspension of 4×10^6 CFU/mL in RPMI-1640 an equal volume of 100% FBS was added and the final cell density was 2×10^6 CFU/mL. To the wells of a 96-well polystyrene plate, 50 μL of 5 μM AMB and 400 μM Os−C(W_5) in RPMI-1640-50% FBS were added. Then, 50 μL of the cell suspension was added followed by incubation for 24 h at 37 °C without shaking. The final concentrations of AMB and Os−C(W_5) were 2.5 μM and 200 μM, respectively.

Likewise, for biofilm eradication, the cell density was 2×10^6 CFU/mL in RPMI-1640 and following the addition of FBS was reduced to 1×10^6 CFU/mL in RPMI-1640-50% FBS. A 100 μL volume of the cell suspension was added to the wells of a 96-well polystyrene plate, and the cells were incubated for 24 h at 37 °C without shaking. The medium was removed, and the established biofilms were rinsed with 100 μL of PBS. Then, 100 μL of AMB (2.5 μM) and 400 μM Os−C(W_5) prepared in RPMI-1640-50% FBS were added to biofilms followed by incubation for another 24 h at 37 °C without shaking.

For both biofilm prevention and eradication studies, the viability and biomass were quantified using CTB and crystal violet (CV), respectively. Biofilm viability was determined by adding 100 μL of a 1/10 dilution of CTB to each well, followed by incubation for 1 h in the dark. Fluorescence was measured at an Ex of 535 nm and an Em of 590 nm. Biofilm biomass was quantified by using CV staining. Biofilms were fixed with 100 μL of 20% (v/v) formaldehyde for 15 min at room temperature. The fixative was removed, and the biofilms were left to dry for a few minutes before 200 μL of 0.1% (w/v) CV was added for 15 min at room temperature. The CV was then removed, and the biofilms were rinsed with 200 μL of ddH_2O to remove unbound CV. The plates were dried overnight, and then the biofilms were viewed using an inverted light microscope equipped with a camera (Optika; Ponteranica, Italy). To quantify staining, the CV was solubilized with 125 μL of a 30% (v/v) acetic acid solution for 15 min. Biomass was quantified by measuring the absorbance of the solubilized CV at 550 nm.

Hemolytic Activity. For the hemolysis assay, blood (single donor per assay) was collected from healthy, consenting donors (ethical clearance; protocol no. 367/2021, Research Ethics Committee, Faculty of Health Sciences, University of Pretoria). The hemolytic activity of Os−C(W_5) was determined as detailed by Nakajima et al.[74] Briefly, from whole blood, erythrocytes were collected by centrifugation, washed, and diluted in PBS, pH 7.4. A 5% erythrocyte suspension was incubated with Os−C(W_5) (0.78−100 μM) for 30 min at 37 °C and 5% CO_2. After incubation, erythrocytes were pelleted via centrifugation, the supernatants were transferred to a 96-well plate, and the absorbance was measured at 570 nm. Sodium dodecyl sulfate (2%) was used as a positive control.

Planktonic: Mode of Action Studies. *SYTOX Green Uptake Assay.* Membrane permeabilization was investigated as described by Merlino et al.,[75] with some modifications. Briefly, cells were resuspended in ddH_2O and then diluted to a cell density of 1×10^7 CFU/mL. An equal volume of SYTOX Green (Invitrogen; Waltham, Massachusetts, USA) prepared in 0.02 M NaP buffer, pH 7.4, was added to the cells to obtain a cell density of 5×10^6 CFU/mL and a SYTOX Green concentration of 1 μM. The suspension was incubated in the dark for 50 min at 30 °C with shaking at 150 rpm to allow for dye equilibration followed by the addition of 50 μL of the suspension to 50 μL of 0.625 μM and 1.25 μM AMB or 6.25−100 μM Os−C(W_5) in the wells of a black 96-well plate (Nunc; Roskilde, Denmark). The final concentrations of AMB and Os−C(W_5) were 0.312−0.625 μM and 3.12−50 μM, respectively. After 3 h of incubation at 37 °C, the fluorescence

https://doi.org/10.1021/acsomega.4c00478
ACS Omega 2024, 9, 15556−15572

was measured at Ex and Em of 485 and 535 nm, respectively. Isopropanol (6.25%) was used as a positive control.

2′,7′-Dichlorodihydrofluorescin Diacetate Assay. Reactive oxygen species production was investigated using the fluorescent dye DCFH-DA and was performed under the same conditions as those described for the SYTOX Green assay with some modifications. Briefly, *C. albicans* cells were resuspended and then diluted to a cell density of 1×10^7 CFU/mL. Equal volumes of the cell suspension and 40 μM DCFH-DA were mixed and then incubated in the dark for 30 min at 37 °C with shaking at 150 rpm. Os−C(W_5) (6.25−50 μM) with and without 10 mM ascorbic acid (Sigma-Aldrich; St Louis, Missouri, USA) was prepared and added to the wells of a black 96-well plate. Cells (50 μL) were added to 50 μL of Os−C(W_5) to give a final peptide concentration range of 3.12−25 μM, and fluorescence was measured every hour for 3 h at an Ex and Em of 485 and 535 nm, respectively. Hydrogen peroxide (2 mM) was used as a positive control. To determine whether ROS production was linked to antifungal activity, cells were exposed to Os−C and Os−C(W_5) (final concentration: 3.12−25 μM) for 3 h in the absence and presence of 10 mM ascorbic acid. Cell viability was determined using CTB as described for antiplanktonic assays.

Scanning Electron Microscopy. Cells were treated for 3 h with 6.25−12.5 μM Os−C(W_5) in 96-well polypropylene plates before being transferred to poly-L-lysine coated coverslips. Samples were fixed with 2.5% glutaraldehyde/formaldehyde and then underwent post fixation with 1% osmium tetroxide. Using 30, 50, 70, 90, and 100% ethanol, the samples were dehydrated and then dried overnight in hexamethyldisilane. Samples were mounted with carbon tape onto aluminum stubs, carbon coated, and viewed with an Ultra plus field emission gun scanning electron microscope (Zeiss; Oberkochen, Germany).

Biofilm: Mode of Action Studies. *Adhesion Assay.* The adhesion assay was performed by adding 50 μL of the cell suspension (2×10^6 CFU/mL) to 50 μL of 0.156 μM AMB or 1.25−20 μM Os−C(W_5) in the wells of a sterile, 96-well polystyrene plate. The final concentration of AMB was 0.078 μM, while the final concentration of Os−C(W_5) ranged from 0.625−10 μM. After 1 h incubation at 37 °C without shaking, the nonadherent cells were removed by washing with PBS. Adherent cells were quantified using the CV assay as described for antibiofilm assays.

Biochemical Analysis of ECM Carbohydrates, Proteins, and Nucleic Acids. Changes in the ECM composition induced by AMB and Os−C(W_5) were determined by performing biofilm prevention assays for 24 h. PBS (200 μL) was added to each well, and then the biofilms were dislodged from the plate surface with a sterile pipet tip. To further disrupt the biofilm, the plate was vortexed for 30 s and then was subjected to a further 15 min of sonication using a Bransonic42 water bath sonicator (Branson Ultrasonics; Brookfield, Connecticut, USA) followed by a final vortexing for 30 s. The suspensions were transferred to microcentrifuge tubes and then centrifuged for 10 min at 13,800 × *g*, and the collected supernatants were used to determine the carbohydrate, protein, and nucleic acid contents.

Carbohydrates were measured using the phenol-sulfuric acid method by Masuko et al.[76] The supernatant was added to a 96-well plate followed by the addition of 150 μL of concentrated sulfuric acid and 30 μL of 5% phenol. After incubation for 5 min at 90 °C in a water bath, the samples were cooled to room temperature before the absorbance was measured at 490 nm. The carbohydrate content was calculated using a glucose standard curve. The protein content was measured using the bicinchoninic acid assay (Thermo Fisher Scientific; Waltham, Massachusetts, USA) according to the manufacturer's instructions, with bovine serum albumin used to generate a standard curve. Finally, the nucleic acid content was determined as described by Hammer et al.[77] by measuring the absorbance of the supernatant at 260 nm, except the samples were not filtered prior to measuring the absorbance.

Statistical Analysis. Three biological repeats were performed in triplicate for all assays, and the results were expressed as the mean ± SEM. Statistical analysis was performed using GraphPad Prism 7 (San Diego, California, USA). ANOVA was performed followed by a posthoc multiple comparisons test. A p-value of <0.05 was used to indicate significance: *$p < 0.05$; **$p < 0.01$; ***$p < 0.001$; ****$p < 0.0001$.

■ ASSOCIATED CONTENT

Data Availability Statement

All data supporting the findings of this study are available in the figures and Supporting Information.

Supporting Information

The Supporting Information is available free of charge at https://pubs.acs.org/doi/10.1021/acsomega.4c00478.

Effect of antifungal agents on cell growth and viability; biofilm preventing activity of AMB, Os−C, and Os−C(W_5); biofilm eradicating activity of AMB and Os−C(W_5); microscopy images of cells exposed to AMB; and HPLC and MS data for Os−C and Os−C(W_5) (PDF)

■ AUTHOR INFORMATION

Corresponding Author

Anabella R. M. Gaspar − *Department of Biochemistry, Genetics and Microbiology, Faculty of Natural and Agricultural Sciences, University of Pretoria, Pretoria 0002, South Africa;* orcid.org/0000-0003-2035-3084; Email: anabella.gaspar@up.ac.za

Authors

Court K. Chiramba − *Department of Biochemistry, Genetics and Microbiology, Faculty of Natural and Agricultural Sciences, University of Pretoria, Pretoria 0002, South Africa*

Dalton S. Möller − *Department of Biochemistry, Genetics and Microbiology, Faculty of Natural and Agricultural Sciences, University of Pretoria, Pretoria 0002, South Africa*

Christian D. Lorenz − *Department of Physics, King's College London, London WC2R 2LS, U.K.;* orcid.org/0000-0003-1028-4804

Rumbidzai R. Chirombo − *Department of Anatomy, Faculty of Health Sciences, University of Pretoria, Pretoria 0002, South Africa*

A. James Mason − *Institute of Pharmaceutical Science, School of Cancer & Pharmaceutical Science, King's College London, London SE1 9NH, U.K.;* orcid.org/0000-0003-0411-602X

Megan J. Bester − *Department of Anatomy, Faculty of Health Sciences, University of Pretoria, Pretoria 0002, South Africa*

Complete contact information is available at: https://pubs.acs.org/10.1021/acsomega.4c00478

https://doi.org/10.1021/acsomega.4c00478
ACS Omega 2024, 9, 15556−15572

Author Contributions

C.K.C. performed all experiments except the hemolysis assay which was performed by R.R.C. A.R.M.G. and M.J.B. conceptualized the study. C.K.C. wrote the main manuscript text and together with A.R.M.G., M.J.B, D.S.M, C.D.L., and A.J.M. prepared the final draft. C.K.C., D.S.M., C.D.L., and A.J.M. designed, performed, and/or analyzed the atomistic simulation data.

Notes

The authors declare no competing financial interest.

■ ACKNOWLEDGMENTS

We hereby acknowledge the National Research Foundation and the University of Pretoria for their financial support. This study was made possible through the capacity built and supported by the SA-UK Newton Fund Antibiotic Accelerator (MC_PC_MR/T029552/1), awarded to A.J.M. and A.R.M.G., and administered by the Medical Research Council (MRC) and the South African Medical Research Council (SAMRC). We thank Prof Yasien Sayed and Keiran Mcinnes from the Protein Structure−Function Research Unit at the University of the Witwatersrand for their assistance with CD experiments. We also extend our thanks to the staff of the Laboratory for Microscopy and Microanalysis at the University of Pretoria for the use of the scanning electron microscope. We are grateful to the UK Materials and Molecular Modelling Hub, which is partially funded by EPSRC (EP/P020194/1 and EP/T022213/1), and the UK HPC Materials Chemistry Consortium, which is also funded by EPSRC (EP/R029431), for providing us access to computational resources. This work also benefited from access to the King's Computational Research, Engineering and Technology Environment (CREATE) at King's College London.[78]

■ ABBREVIATIONS

AMP, antimicrobial peptide; ECM, extracellular matrix; NaP, sodium phosphate; ddH_2O, double-distilled water; AMB, amphotericin B; POPC, 1-palmitoyl-2-oleoyl-*sn*-glycero-3-phosphocholine; POPE, 1-palmitoyl-2-oleoyl-*sn*-glycero-3-phosphoethanolamine; POPS, 1-palmitoyl-2-oleoyl-*sn*-glycero-3-phospho-L-serine; POPI, 1-palmitoyl-2-oleoyl-*sn*-glycero-3-phosphoinositol; YPD, yeast peptone dextrose; CTB, CellTiter Blue; CV, crystal violet; DCFH-DA, 2′,7′-dichlorodihydrofluorescin diacetate; FBS, fetal bovine serum

■ REFERENCES

(1) World Health Organisation; *WHO fungal priority pathogens list to guide research, development and public health action*, 2022.
(2) Pappas, P. G.; Lionakis, M. S.; Arendrup, M. C.; Ostrosky-Zeichner, L.; Kullberg, B. J. Invasive candidiasis. *Nature Reviews Disease Primers.* **2018**, *4*, 18026−18045.
(3) Denning, D. W. Antifungal drug resistance: an update. *European Journal of Hospital Pharmacy* **2022**, *29* (2), 109−112.
(4) Mnge, P.; Okeleye, B. I.; Vasaikar, S. D.; Apalata, T. Species distribution and antifungal susceptibility patterns of *Candida* isolates from a public tertiary teaching hospital in the Eastern Cape Province, South Africa. *Braz. J. Med. Biol. Res.* **2017**, *50* (6), e5797−e5803.
(5) Mulu, A.; Kassu, A.; Anagaw, B.; Moges, B.; Gelaw, A.; Alemayehu, M.; Belyhun, Y.; Biadglegne, F.; Hurissa, Z.; Moges, F.; Isogai, E. Frequent detection of 'azole' resistant *Candida* species among late presenting AIDS patients in northwest Ethiopia. *BMC Infectious Diseases.* **2013**, *13* (82), 1−10.
(6) Dos Santos Abrantes, P. M.; McArthur, C. P.; Africa, C. W. Multi-drug resistant oral *Candida* species isolated from HIV-positive patients in South Africa and Cameroon. *Diagnostic Microbiology and Infectious Disease.* **2014**, *79* (2), 222−227.
(7) World Health Organisation; *Global action plan on antimicrobial resistance*, 2015.
(8) Sanguinetti, M.; Posteraro, B.; Lass-Florl, C. Antifungal drug resistance among *Candida* species: mechanisms and clinical impact. *Mycoses.* **2015**, *58*, 2−13.
(9) Mitchell, K. F.; Zarnowski, R.; Andes, D. R. Fungal super glue: the biofilm matrix and its composition, assembly, and functions. *PLoS Pathogens.* **2016**, *12* (9), e1005828−e1005833.
(10) Bahar, A. A.; Ren, D. Antimicrobial peptides. *Pharmaceuticals (Basel).* **2013**, *6* (12), 1543−1575.
(11) Brogden, K. A. Antimicrobial peptides: pore formers or metabolic inhibitors in bacteria? *Nature Reviews Microbiology.* **2005**, *3* (3), 238−250.
(12) Mookherjee, N.; Anderson, M. A.; Haagsman, H. P.; Davidson, D. J. Antimicrobial host defence peptides: functions and clinical potential. *Nat. Rev. Drug Discovery* **2020**, *19* (5), 311−332.
(13) Thompson, G. R.; Soriano, A.; Skoutelis, A.; Vazquez, J. A.; Honore, P. M.; Horcajada, J. P.; Spapen, H.; Bassetti, M.; Ostrosky-Zeichner, L.; Das, A. F.; Viani, R. M.; Sandison, T.; Pappas, P. G. Rezafungin versus caspofungin in a phase 2, randomized, double-blind study for the treatment of candidemia and invasive candidiasis: the STRIVE trial. *Clinical Infectious Diseases* **2021**, *73* (11), e3647−e3655.
(14) Marr, A. K.; Gooderham, W. J.; Hancock, R. E. W. Antibacterial peptides for therapeutic use: obstacles and realistic outlook. *Current Opinion in Pharmacology.* **2006**, *6* (5), 468−472.
(15) Yu, H. Y.; Tu, C. H.; Yip, B. S.; Chen, H. L.; Cheng, H. T.; Huang, K. C.; Lo, H. J.; Cheng, J. W. Easy strategy to increase salt resistance of antimicrobial peptides. *Antimicrob. Agents Chemother.* **2011**, *55* (10), 4918−4921.
(16) Pasupuleti, M.; Schmidtchen, A.; Chalupka, A.; Ringstad, L.; Malmsten, M. End-tagging of ultra-short antimicrobial peptides by W/F stretches to facilitate bacterial killing. *PLoS One.* **2009**, *4* (4), e5285−e5294.
(17) Schmidtchen, A.; Pasupuleti, M.; Morgelin, M.; Davoudi, M.; Alenfall, J.; Chalupka, A.; Malmsten, M. Boosting antimicrobial peptides by hydrophobic oligopeptide end tags. *J. Biol. Chem.* **2009**, *284* (26), 17584−17594.
(18) Pasupuleti, M.; Chalupka, A.; Morgelin, M.; Schmidtchen, A.; Malmsten, M. Tryptophan end-tagging of antimicrobial peptides for increased potency against *Pseudomonas aeruginosa*. *Biochim. Biophys. Acta* **2009**, *1790* (8), 800−808.
(19) Schmidtchen, A.; Ringstad, L.; Kasetty, G.; Mizuno, H.; Rutland, M. W.; Malmsten, M. Membrane selectivity by W-tagging of antimicrobial peptides. *Biochim. Biophys. Acta* **2011**, *1808* (4), 1081−1091.
(20) Strömstedt, A. A.; Pasupuleti, M.; Schmidtchen, A.; Malmsten, M. Oligotryptophan-tagged antimicrobial peptides and the role of the cationic sequence. *Biochimica et Biophysica Acta (BBA) -. Biomembranes* **2009**, *1788* (9), 1916−1923.
(21) Sonesson, A.; Nordahl, E. A.; Malmsten, M.; Schmidtchen, A. Antifungal activities of peptides derived from domain 5 of high-molecular-weight kininogen. *Int. J. Pept.* **2011**, *2011*, No. 761037.
(22) Prinsloo, L.; Naidoo, A.; Serem, J. C.; Taute, H.; Sayed, Y.; Bester, M. J.; Neitz, A. W. H.; Gaspar, A. R. M. Structural and functional characterization of peptides derived from the carboxy-terminal region of a defensin from the tick *Ornithodoros savignyi*. *Journal of Peptide Science.* **2013**, *19* (5), 325−332.
(23) Taute, H.; Bester, M. J.; Neitz, A. W. H.; Gaspar, A. R. M. Investigation into the mechanism of action of the antimicrobial peptides Os and Os-C derived from a tick defensin. *Peptides* **2015**, *71*, 179−187.
(24) Mbuayama, K. R.; Taute, H.; Strömstedt, A. A.; Bester, M. J.; Gaspar, A. R. M. Antifungal activity and mode of action of synthetic peptides derived from the tick OsDef2 defensin. *J. Pept. Sci.* **2021**, *28* (5), No. e3383.
(25) Freskgard, P. O.; Martensson, L. G.; Jonasson, P.; Jonsson, B. H.; Carlsson, U. Assignment of the contribution of the tryptophan

https://doi.org/10.1021/acsomega.4c00478
ACS Omega 2024, 9, 15556−15572

residues to the circular dichroism spectrum of human carbonic anhydrase II. *Biochemistry* **1994**, *33* (47), 14281−14288.
(26) Reeb, J.; Rost, B. Secondary structure prediction. *Encyclopedia of Bioinformatics and Computational Biology* **2019**, *2*, 488−496.
(27) Johnston, A. J.; Zhang, Y. R.; Busch, S.; Pardo, L. C.; Imberti, S.; McLain, S. E. Amphipathic solvation of indole: implications for the role of tryptophan in membrane proteins. *J. Phys. Chem. B* **2015**, *119* (19), 5979−5987.
(28) Manzo, G.; Ferguson, P. M.; Gustilo, V. B.; Hind, C. K.; Clifford, M.; Bui, T. T.; Drake, A. F.; Atkinson, R. A.; Sutton, J. M.; Batoni, G.; Lorenz, C. D.; Phoenix, D. A.; Mason, A. J. Minor sequence modifications in temporin B cause drastic changes in antibacterial potency and selectivity by fundamentally altering membrane activity. *Scientific Reports.* **2019**, *9* (1), 1385−1400.
(29) Manzo, G.; Hind, C. K.; Ferguson, P. M.; Amison, R. T.; Hodgson-Casson, A. C.; Ciazynska, K. A.; Weller, B. J.; Clarke, M.; Lam, C.; Man, R. C. H.; Shaughnessy, B. G. O.; Clifford, M.; Bui, T. T.; Drake, A. F.; Atkinson, R. A.; Lam, J. K. W.; Pitchford, S. C.; Page, C. P.; Phoenix, D. A.; Lorenz, C. D.; Sutton, J. M.; Mason, A. J. A pleurocidin analogue with greater conformational flexibility, enhanced antimicrobial potency and *in vivo* therapeutic efficacy. *Communications Biology.* **2020**, *3* (1), 697−712.
(30) Zai, Y.; Xi, X.; Ye, Z.; Ma, C.; Zhou, M.; Chen, X.; Siu, S. W. I.; Chen, T.; Wang, L.; Kwok, H. F. Aggregation and its influence on the bioactivities of a novel antimicrobial peptide, temporin-PF, and its analogues. *Int. J. Mol. Sci.* **2021**, *22* (9), 4509.
(31) Sarig, H.; Rotem, S.; Ziserman, L.; Danino, D.; Mor, A. Impact of self-assembly properties on antibacterial activity of short acyl-lysine oligomers. *Antimicrobial Agents and Chemotherapy.* **2008**, *52* (12), 4308−4314.
(32) Lace, I.; Cotroneo, E. R.; Hesselbarth, N.; Simeth, N. A. Artificial peptides to induce membrane denaturation and disruption and modulate membrane composition and fusion. *Journal of Peptide Science* **2023**, *29* (5), e3466−e3495.
(33) Sengupta, D.; Leontiadou, H.; Mark, A. E.; Marrink, S. J. Toroidal pores formed by antimicrobial peptides show significant disorder. *Biochim. Biophys. Acta* **2008**, *1778* (10), 2308−2317.
(34) Ciornei, C. D.; Sigurdardottir, T.; Schmidtchen, A.; Bodelsson, M. Antimicrobial and chemoattractant activity, lipopolysaccharide neutralization, cytotoxicity, and inhibition by serum of analogs of human cathelicidin LL-37. *Antimicrob. Agents Chemother.* **2005**, *49* (7), 2845−2850.
(35) Lee, D. Y.; Lee, S. Y.; Yun, S. H.; Jeong, J. W.; Kim, J. H.; Kim, H. W.; Choi, J. S.; Kim, G. D.; Joo, S. T.; Choi, I.; Hur, S. J. Review of the current research on fetal bovine serum and the development of cultured meat. *Food Science of Animal Resources* **2022**, *42* (5), 775−799.
(36) Hein-Kristensen, L.; Knapp, K. M.; Franzyk, H.; Gram, L. Selectivity in the potentiation of antibacterial activity of α-peptide/β-peptoid peptidomimetics and antimicrobial peptides by human blood plasma. *Research in Microbiology* **2013**, *164* (9), 933−940.
(37) Lai, Z.; Yuan, X.; Chen, H.; Zhu, Y.; Dong, N.; Shan, A. Strategies employed in the design of antimicrobial peptides with enhanced proteolytic stability. *Biotechnology Advances* **2022**, *59*, 107962−107981.
(38) Ebenhan, T.; Gheysens, O.; Kruger, H. G.; Zeevaart, J. R.; Sathekge, M. M. Antimicrobial peptides: their role as infection-selective tracers for molecular imaging. *Biomed Res. Int.* **2014**, *2014*, No. 867381.
(39) D'Auria, F. D.; Casciaro, B.; De Angelis, M.; Marcocci, M. E.; Palamara, A. T.; Nencioni, L.; Mangoni, M. L. Antifungal activity of the frog skin peptide temporin G and its effect on *Candida albicans* virulence factors. *Int. J. Mol. Sci.* **2022**, *23* (11), 6345.
(40) Struyfs, C.; Cammue, B. P. A.; Thevissen, K. Membrane-interacting antifungal peptides. *Frontiers in Cell and Developmental Biology* **2021**, *9*, 649875−649891.
(41) Bellavita, R.; Maione, A.; Merlino, F.; Siciliano, A.; Dardano, P.; De Stefano, L.; Galdiero, S.; Galdiero, E.; Grieco, P.; Falanga, A. Antifungal and antibiofilm activity of cyclic temporin L peptide analogues against *albicans* and non-*albicans Candida* species. *Pharmaceutics* **2022**, *14* (2), 454.
(42) Natarajan, A.; Rangan, K.; Vadrevu, R. Self-assembly of a peptide sequence, EKKE, composed of exclusively charged amino acids: Role of charge in morphology and lead binding. *Journal of Peptide Science* **2023**, *29* (2), e3451−e3460.
(43) Jia, F.; Wang, J.; Peng, J.; Zhao, P.; Kong, Z.; Wang, K.; Yan, W.; Wang, R. The *in vitro*, *in vivo* antifungal activity and the action mode of Jelleine-I against *Candida* species. *Amino Acids.* **2018**, *50* (2), 229−239.
(44) Peng, C.; Liu, Y.; Shui, L.; Zhao, Z.; Mao, X.; Liu, Z. Mechanisms of action of the antimicrobial peptide cecropin in the killing of *Candida albicans*. *Life (Basel)* **2022**, *12* (10), 1581.
(45) Pereira, C.; Silva, R. D.; Saraiva, L.; Johansson, B.; Sousa, M. J.; Corte-Real, M. Mitochondria-dependent apoptosis in yeast. *Biochim. Biophys. Acta* **2008**, *1783* (7), 1286−1302.
(46) Curtin, J. F.; Donovan, M.; Cotter, T. G. Regulation and measurement of oxidative stress in apoptosis. *Journal of Immunological Methods* **2002**, *265*, 49−72.
(47) Morita, M.; Yano, S.; Yamaguchi, T.; Sugimoto, T. Advanced glycation end products-induced reactive oxygen species generation is partly through NF-kappa B activation in human aortic endothelial cells. *Journal of Diabetes and Its Complications* **2013**, *27* (1), 11−15.
(48) Ma, H.; Yang, L.; Tian, Z.; Zhu, L.; Peng, J.; Fu, P.; Xiu, J.; Guo, G. Antimicrobial peptide AMP-17 exerts anti-*Candida albicans* effects through ROS-mediated apoptosis and necrosis. *International Microbiology* **2023**, *26* (1), 81−90.
(49) Cools, T. L.; Struyfs, C.; Drijfhout, J. W.; Kucharikova, S.; Lobo Romero, C.; Van Dijck, P.; Ramada, M. H. S.; Bloch, C., Jr.; Cammue, B. P. A.; Thevissen, K. A linear 19-mer plant defensin-derived peptide acts synergistically with caspofungin against *Candida albicans* biofilms. *Frontiers in Microbiology* **2017**, *8*, 2051−2064.
(50) Aerts, A. M.; Bammens, L.; Govaert, G.; Carmona-Gutierrez, D.; Madeo, F.; Cammue, B. P. A.; Thevissen, K. The antifungal plant defensin HsAFP1 from *Heuchera sanguinea* induces apoptosis in *Candida albicans*. *Frontiers in Microbiology* **2011**, *2*, 47−55.
(51) Hayes, B. M. E.; Bleackley, M. R.; Wiltshire, J. L.; Anderson, M. A.; Traven, A.; van der Weerden, N. L. Identification and mechanism of action of the plant defensin NaD1 as a new member of the antifungal drug arsenal against *Candida albicans*. *Antimicrob. Agents Chemother.* **2013**, *57* (8), 3667−3675.
(52) Hayes, B. M. E.; Bleackley, M. R.; Anderson, M. A.; van der Weerden, N. L. The plant defensin NaD1 enters the cytoplasm of *Candida albicans* via endocytosis. *J. Fungi (Basel)* **2018**, *4* (1), 20.
(53) Thevissen, K.; de Mello Tavares, P.; Xu, D.; Blankenship, J.; Vandenbosch, D.; Idkowiak-Baldys, J.; Govaert, G.; Bink, A.; Rozental, S.; de Groot, P. W.; Davis, T. R.; Kumamoto, C. A.; Vargas, G.; Nimrichter, L.; Coenye, T.; Mitchell, A.; Roemer, T.; Hannun, Y. A.; Cammue, B. P. A. The plant defensin RsAFP2 induces cell wall stress, septin mislocalization and accumulation of ceramides in *Candida albicans*. *Mol. Microbiol.* **2012**, *84* (1), 166−180.
(54) Yu, Q.; Zhang, B.; Li, J.; Zhang, B.; Wang, H.; Li, M. Endoplasmic reticulum-derived reactive oxygen species (ROS) is involved in toxicity of cell wall stress to *Candida albicans*. *Free Radical Biol. Med.* **2016**, *99*, 572−583.
(55) Ramírez-Quijas, M. D.; Zazueta-Sandoval, R.; Obregón-Herrera, A.; López-Romero, E.; Cuéllar-Cruz, M. Effect of oxidative stress on cell wall morphology in four pathogenic *Candida* species. *Mycological Progress.* **2015**, *14* (3), 1−15.
(56) Nikapitiya, C.; Dananjaya, S. H. S.; Chandrarathna, H. P. S. U.; De Zoysa, M.; Whang, I. Octominin: a novel synthetic anticandidal peptide derived from defense protein of *Octopus minor*. *Mar. Drugs* **2020**, *18* (1), 56.
(57) Lyu, Y.; Yang, Y.; Lyu, X.; Dong, N.; Shan, A. Antimicrobial activity, improved cell selectivity and mode of action of short PMAP-36-derived peptides against bacteria and *Candida*. *Scientific Reports.* **2016**, *6*, 27258−27269.
(58) Nobile, C. J.; Johnson, A. D. *Candida albicans* biofilms and human disease. *Annual Reviews of Microbiology.* **2015**, *69*, 71−92.

https://doi.org/10.1021/acsomega.4c00478
ACS Omega 2024, 9, 15556−15572

(59) Chang, H. T.; Tsai, P. W.; Huang, H. H.; Liu, Y. S.; Chien, T. S.; Lan, C. Y. LL37 and hBD-3 elevate the beta-1,3-exoglucanase activity of *Candida albicans* Xog1p, resulting in reduced fungal adhesion to plastic. *Biochemistry Journal.* **2012**, *441* (3), 963−970.
(60) Scarsini, M.; Tomasinsig, L.; Arzese, A.; D'Este, F.; Oro, D.; Skerlavaj, B. Antifungal activity of cathelicidin peptides against planktonic and biofilm cultures of *Candida* species isolated from vaginal infections. *Peptides.* **2015**, *71*, 211−221.
(61) Brauner, A.; Alvendal, C.; Chromek, M.; Stopsack, K. H.; Ehrstrom, S.; Schroder, J. M.; Bohm-Starke, N. Psoriasin, a novel anti-*Candida albicans* adhesin. *Journal of Molecular Medicine.* **2018**, *96* (6), 537−545.
(62) Gupta, P.; Gupta, S.; Sharma, M.; Kumar, N.; Pruthi, V.; Poluri, K. M. Effectiveness of phytoactive molecules on transcriptional expression, biofilm matrix, and cell wall components of *Candida glabrata* and its clinical isolates. *ACS Omega.* **2018**, *3* (9), 12201−12214.
(63) Fonseca, E.; Silva, S.; Rodrigues, C. F.; Alves, C. T.; Azeredo, J.; Henriques, M. Effects of fluconazole on *Candida glabrata* biofilms and its relationship with ABC transporter gene expression. *Biofouling.* **2014**, *30* (4), 447−457.
(64) Zarnowski, R.; Sanchez, H.; Covelli, A. S.; Dominguez, E.; Jaromin, A.; Bernhardt, J.; Mitchell, K. F.; Heiss, C.; Azadi, P.; Mitchell, A.; Andes, D. R. *Candida albicans* biofilm-induced vesicles confer drug resistance through matrix biogenesis. *PLoS Biology* **2018**, *16* (10), e2006872−e2006889.
(65) Martins, M.; Uppuluri, P.; Thomas, D. P.; Cleary, I. A.; Henriques, M.; Lopez-Ribot, J. L.; Oliveira, R. Presence of extracellular DNA in the *Candida albicans* biofilm matrix and its contribution to biofilms. *Mycopathologia.* **2010**, *169* (5), 323−331.
(66) Louis-Jeune, C.; Andrade-Navarro, M. A.; Perez-Iratxeta, C. Prediction of protein secondary structure from circular dichroism using theoretically derived spectra. *Proteins* **2012**, *80* (2), 374−381.
(67) Abraham, M. J.; Murtola, T.; Schulz, R.; Páll, S.; Smith, J. C.; Hess, B.; Lindahl, E. GROMACS: high performance molecular simulations through multi-level parallelism from laptops to supercomputers. *SoftwareX.* **2015**, *1−2*, 19−25.
(68) Best, R. B.; Zhu, X.; Shim, J.; Lopes, P. E.; Mittal, J.; Feig, M.; Mackerell, A. D., Jr Optimization of the additive CHARMM all-atom protein force field targeting improved sampling of the backbone phi, psi and side-chain χ_1 and χ_2 dihedral angles. *Journal of Chemical Theory and Computation.* **2012**, *8* (9), 3257−3273.
(69) Huang, J.; MacKerell, A. D., Jr CHARMM36 all-atom additive protein force field: validation based on comparison to NMR data. *Journal of Chemical Theory and Computation.* **2013**, *34* (25), 2135−2145.
(70) Lee, J.; Cheng, X.; Swails, J. M.; Yeom, M. S.; Eastman, P. K.; Lemkul, J. A.; Wei, S.; Buckner, J.; Jeong, J. C.; Qi, Y.; Jo, S.; Pande, V. S.; Case, D. A.; Brooks, C. L.; MacKerell, A. D., Jr; Klauda, J. B.; Im, W. CHARMM-GUI input generator for NAMD, GROMACS, AMBER, OpenMM, and CHARMM/OpenMM simulations using the CHARMM36 additive force field. *Journal of Chemical Theory and Computation.* **2016**, *12* (1), 405−413.
(71) Aguiar, F. L. L.; Santos, N. C.; de Paula Cavalcante, C. S.; Andreu, D.; Baptista, G. R.; Goncalves, S. Antibiofilm activity on *Candida albicans* and mechanism of action on biomembrane models of the antimicrobial peptide Ctn[15−34]. *Int. J. Mol. Sci.* **2020**, *21* (21), 8339.
(72) Warschawski, D. E.; Arnold, A. A.; Beaugrand, M.; Gravel, A.; Chartrand, E.; Marcotte, I. Choosing membrane mimetics for NMR structural studies of transmembrane proteins. *Biochim. Biophys. Acta* **2011**, *1808* (8), 1957−1974.
(73) Rodriguez-Tudela, J. L.; Arendrup, M. C.; Barchiesi, F.; Bille, J.; Chryssanthou, E.; Cuenca-Estrella, M.; Dannaoui, E.; Denning, D. W.; Donnelly, J. P.; Dromer, F.; Fegeler, W.; Lass-Florl, C.; Moore, C.; Richardson, M.; Sandven, P.; Velegraki, A.; Verweij, P. EUCAST definitive document EDef 7.1: method for the determination of broth dilution MICs of antifungal agents for fermentative yeasts. *Clinical Microbiology and Infection.* **2008**, *14* (4), 398−405.
(74) Nakajima, Y.; Ishibashi, J.; Yukuhiro, F.; Asaoka, A.; Taylor, D.; Yamakawa, M. Antibacterial activity and mechanism of action of tick defensin against Gram-positive bacteria. *Biochimica et Biophysica Acta (BBA) - General Subjects.* **2003**, *1624* (1−3), 125−130.
(75) Merlino, F.; Carotenuto, A.; Casciaro, B.; Martora, F.; Loffredo, M. R.; Di Grazia, A.; Yousif, A. M.; Brancaccio, D.; Palomba, L.; Novellino, E.; Galdiero, M.; Iovene, M. R.; Mangoni, M. L.; Grieco, P. Glycine-replaced derivatives of [Pro(3),DLeu(9)]TL, a temporin L analogue: evaluation of antimicrobial, cytotoxic and hemolytic activities. *Eur. J. Med. Chem.* **2017**, *139*, 750−761.
(76) Masuko, T.; Minami, A.; Iwasaki, N.; Majima, T.; Nishimura, S.; Lee, Y. C. Carbohydrate analysis by a phenol-sulfuric acid method in microplate format. *Anal. Biochem.* **2005**, *339* (1), 69−72.
(77) Hammer, K. A.; Carson, C. F.; Riley, T. V. Antifungal effects of *Melaleuca alternifolia* (tea tree) oil and its components on *Candida albicans, Candida glabrata* and *Saccharomyces cerevisiae. J. Antimicrob. Chemother.* **2004**, *53* (6), 1081−1085.
(78) King's Computational Research; *Engineering and Technology Environment (CREATE)*. DOI: 10/18742/rnvf-m076 (accessed March 2, 2022).

https://doi.org/10.1021/acsomega.4c00478
ACS Omega 2024, 9, 15556−15572